CD4 Effectors Need to Recognize Antigen Locally to Become Cytotoxic CD4 and Follicular Helper T Cells

Priyadharshini Devarajan[#1], Allen M. Vong[#1], Catherine H. Castonguay[1], Bianca L. Bautista[1], Michael C. Jones[1], Olivia Kugler-Umana[1], Karen A. Kelly[2], Susan L. Swain*[1]

[1] Department of Pathology, University of Massachusetts Medical School, Worcester, MA 01605, USA.

[2] Department of Animal Medicine, University of Massachusetts Medical School, Worcester, MA 01605, USA.

# P.D. and A.M.V. contributed equally to this work.

***Corresponding author:** Susan L. Swain, Department of Pathology, University of Massachusetts Medical School, Worcester, MA 01605, USA.

Phone: 508-856-4494 (office) Email id: susan.swain@umassmed.edu

Running Title: Tissue Effectors require Local Signals from Ag at an Effector Checkpoint

Summary

T follicular helper (T_{FH}) and Cytotoxic CD4 (ThCTL) are tissue-restricted CD4 effector subsets, functionally specialized to mediate optimal Ab production and cytotoxicity of infected cells. Influenza infection generates robust CD4 responses, including lung ThCTL and SLO T_{FH}, that protect against reinfection by variant strains. Antigen (Ag) presentation after infection, lasts through the effector phase of the response. Here, we show that this effector phase Ag presentation, well after priming, is required to drive CD4 effectors to ThCTL and T_{FH}. Using *in vivo* influenza models, we varied Ag presentation to effectors acutely, just at the effector phase. Ag presentation was required in the tissue of effector residence. We suggest these requirements contain unnecessary or potentially pathogenic CD4 responses, only allowing them if infection is uncleared. The results imply that providing effector phase Ag, would lead to stronger humoral and CD4 tissue immunity and thus can be applied to improve vaccine design.

Keywords: Tissue-Restricted, Effectors, Influenza, Pathogen, Vaccination, CD4 T cells, Immunization, T Cytotoxic, T Helper, T_{FH}

INTRODUCTION

A key challenge for the immune system is to respond strongly against dangerous pathogens, while limiting response to non-threatening foreign antigens, so as to limit immunopathology. Naïve CD4 T cells achieve this discrimination by requiring three signals during priming at the beginning of the response to generate the initial effector populations: high levels of antigen (Ag), co-stimulation and inflammatory cytokines (Dubey and Croft, 1996). These effectors defend the body against foreign Ag during the effector phase and finally contract after the Ag has waned to become long lived memory T cells. A cohort of the CD4 effectors can differentiate further, to become tissue-restricted effectors, including T follicular helpers (T_{FH}) (Fazilleau et al., 2009; Lee et al., 2015) and cytotoxic CD4 T cells (ThCTL) (Marshall et al., 2016).

T_{FH} are tissue-restricted CD4 effectors in the secondary lymphoid organs such as the spleen and lymph nodes (Fazilleau et al., 2009; Lee et al., 2015). They drive the germinal center reaction and the resulting antibody (Ab) responses during the immune response (Crotty, 2019). ThCTL are cytotoxic CD4 effectors that target cells expressing MHC-II, which may also have downregulated MHC-I due to evasion mechanisms, and play important roles in controlling viral infections and tumors (Juno et al., 2017; Koutsakos et al., 2019a; Marshall and Swain, 2011; Marshall et al., 2016; Muraro et al., 2017; Phetsouphanh et al., 2017). Previously, we showed that ThCTL induced by viral infections are resident in the infected tissue (Marshall et al., 2016). During influenza virus infection, ThCTL arise 7 days post infection (dpi) in lungs of infected mice. ThCTL express NKG2C/E, which reliably marks the CD4 effector subset with MHC-II restricted cytotoxicity. Both T_{FH} and ThCTL are also upregulated in various human autoimmune diseases (Broadley et al., 2017; Gensous et al., 2018). Despite their important roles in autoimmune disease, infection,

and cancer, little is known about the signals that regulate the transition of early CD4 effectors into these later tissue effectors.

Our current understanding of CD4 tissue-restricted effectors is largely inferred from studies of T_{FH} during T:B interaction in responding germinal centers. Over the past decade we have learned that after priming, T_{FH} repeatedly interact with B cells in germinal centers to support GC responses. The germinal center B cells (GCB) reciprocally support T_{FH} differentiation, survival and expansion (Vinuesa et al., 2016). Studies have shown that T_{FH} generation is enhanced by repeated immunization (Baumjohann et al., 2013; Deenick et al., 2010; Tam et al., 2016), but it is unclear if Ag is required both for initial priming and at the effector phase. CD4 effectors generated during LCMV infection, depended on ongoing infection to effectively generate T_{FH} (Baumjohann et al., 2013). In this study it was unclear whether Ag, or infection-generated inflammation, or both, were required to support T_{FH} generation during the effector phase and if Ag presentation needed to occur in particular locations. While we know that T_{FH} continuously interact with GCB that present Ag *in situ*, we do not know which aspects of this interaction are required <u>during the effector phase</u>, to regulate the development of CD4 tissue effector subsets. Moreover, we do not know if the GC presents a niche, unique in its ability to fulfill requirements for CD4 tissue effector differentiation or if there are other signals that are able to substitute for them. An immunization study indicated that GCB depletion during the effector phase reduced T_{FH} generation (Baumjohann et al., 2013). Another study showed that early T_{FH} generation can occur independently of unique B cell signaling (Deenick et al., 2011), supporting the concept that when other APC presenting Ag are available, T_{FH} may be able to develop by GCB independent pathways even during the effector phase, though this is unknown. Moreover, other CD4 tissue effectors such as ThCTL are not present in GC and we have little understanding of their development from early CD4 effectors, or if they have shared

or unique requirements with T_{FH}. Thus, while the GC studies give us many important clues about CD4 tissue effectors, they leave many questions unanswered. To fill these gaps, here we analyze the overall requirements for different aspects of Ag encounter, specifically during the CD4 effector phase well after priming, that drive CD4 effectors to become tissue-restricted effectors.

We previously showed that CD4 effectors generated by influenza virus infection need to recognize Ag during the effector phase, 6-8 dpi, to effectively form long-lived memory (Bautista et al., 2016; McKinstry et al., 2014). Here, we ask if late steps in generation of T_{FH} and ThCTL tissue effector subsets, also require cognate Ag recognition at this "effector checkpoint". We reason that if an infection is quickly cleared or initial Ag is non-replicating, presentation of Ag will wane. Thus, such a checkpoint could act to limit further response when the infection (the source of Ag) is cleared, serving as a mechanism to prevent immunopathology and potential autoimmunity when there is no longer danger from a live pathogen.

Here, we find that CD4 effectors must recognize cognate Ag during the effector checkpoint to become full-fledged ThCTL and T_{FH}, and that multiple APC can support this transition. Moreover, for full development of DLN T_{FH}, spleen T_{FH} and lung ThCTL, effectors must recognize Ag presented at the site of tissue effector residency. CD28 co-stimulation during the effector checkpoint is required for T_{FH}, but not for ThCTL generation. Thus, at the effector phase, well after Ag priming, multiple signals during cognate Ag recognition act in concert to drive different specialized CD4 fates: ThCTL, T_{FH} and CD4 memory. This suggests that this effector CD4 checkpoint regulates the quality, quantity and localization of CD4 tissue-restricted effectors and the memory cells they become. We discuss the relevance of these findings to designing vaccine

strategies that could induce effective long-lived Ab and cellular immunity against conserved epitopes.

RESULTS

Cognate Ag recognition at the CD4 effector checkpoint drives the generation of ThCTL phenotype and function in the lung

We use a sequential transfer model, in which 6 dpi CD4 effectors are generated *in vivo* by transferring naïve HNT (specific for influenza A virus hemagglutinin) or OT-II (specific for an OVA epitope) Thy1.1 CD4 T cells, into primary hosts infected with PR8 or with PR8-OVA_{II} influenza virus respectively (for 6 days). We then isolate the *in vivo* generated effectors and transfer them into 2nd hosts. The 2nd hosts are IAV infection-matched mice, i.e. also at 6 dpi when 6 dpi effectors are transferred into them, to make the model physiologically relevant. In the 2nd hosts, we can independently modulate Ag availability by using Ag-pulsed APC (Ag/APC) transfers or virus infections. This allows us to clearly follow donor cell fate to ask specific questions about cognate Ag/APC interactions during the effector phase.

In all experiments using the sequential transfer model, we analyze the transferred donor effector cells 2-4 days post transfer (8-10 days post infection) and not later, because ThCTL and T_{FH} peak 7-10 days post infection (Marshall et al., 2016) (Fig S1D-E), and then effectors begin to contract after 10 dpi (Botta et al., 2017; Marshall et al., 2016). Signals required for CD4 T cell priming during the first few days are well-defined (Swain et al., 2012). The sequential transfer model allows us to define signals required during the effector phase, well after priming, but before contraction. Since there is robust generation of both ThCTL and T_{FH} during an *in vivo* influenza infection (Figure S1D-E), they serve as positive controls. Thus an important advantage of this TCR Tg

approach is that we can isolate 6d CD4 effectors generated by *in vivo* influenza infection, then transfer them with added/subtracted signals related to Ag into the 2nd infection matched hosts and analyze tissue effector generation compared with positive controls, to identify required signals.

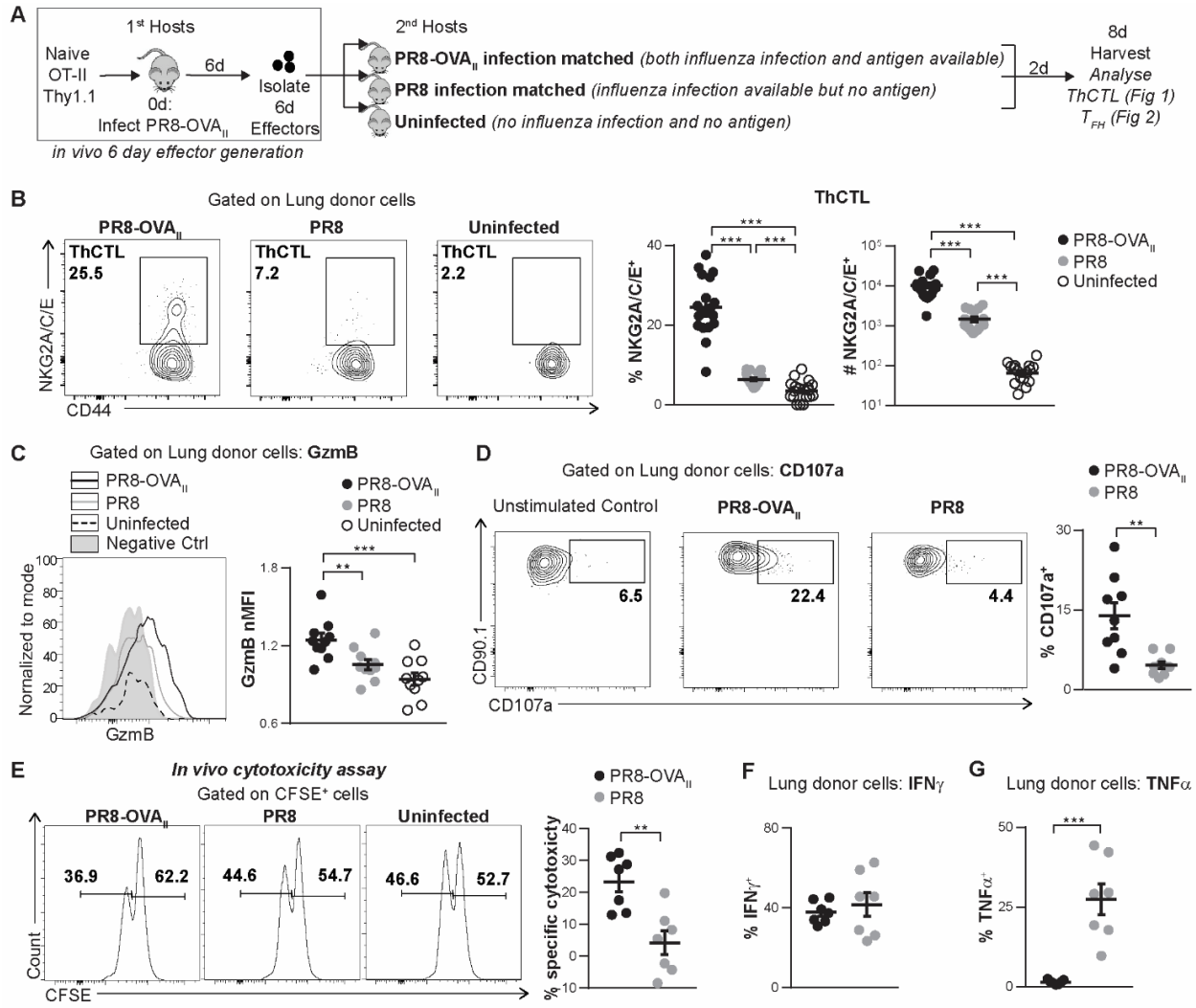

Fig. 1. Cognate Ag during the effector checkpoint is required for lung ThCTL phenotype and function. (A) Experimental design for (B-D): Naïve OT-II.Thy1.1$^+$ cells were transferred into PR8-OVA$_{II}$ infected mice (1st hosts). At 6 dpi, OT-II.Thy1.1$^+$ effectors were isolated from 1st hosts and transferred into following groups of 2nd hosts: 6 dpi PR8-OVA$_{II}$-infected, 6 dpi PR8-infected, or uninfected mice. Donor cells were analyzed 8 dpi. **(B)** Percentage and numbers of donor lung ThCTL (NKG2A/C/E$^+$) (n=19 per group pooled, 4 independent experiments). **(C)** Representative histogram of lung donor cell GzmB expression (negative control: naïve CD4 from uninfected mice). Normalized MFI of lung donor cell GzmB expression (n=10 per group pooled, 2 independent experiments). **(D)** CD107a degranulation marker expression by lung donor cells (n=9 per group pooled, 2 independent experiments). **(E)** Experimental design: *In vivo* 6d OT-II.Thy1.1$^+$ effectors were transferred into 6 dpi PR8-OVA$_{II}$ or PR8 infection-matched TCRα/β$^{-/-}$ mice. CFSE^{lo} target and CFSE^{hi} bystander cells were transferred at 7d. Representative CFSE histograms shown. Percentage Ag specific cytotoxicity in each group is shown. **(F-G)** Experiment done as in (E). Percentage of lung donor cells expressing intracellular IFNγ (F) and TNFα (G) (E-G, n=7 per group pooled, 2 independent experiments). Statistical significance determined by two-tailed, unpaired Student's t-test (* P<0.05, ** P<0.01, *** P<0.001). See also Fig. S2.

We first analyzed if early ThCTL had recently recognized Ag during an *in vivo* influenza infection. For this, we used influenza-specific TCR transgenic CD4 T (OT-II specific for PR8-OVA_{II}) mice crossed to the $Nur77^{GFP}$ reporter mice, as a source of reporter CD4 T cells, to track recent TCR stimulation. $Nur77^{GFP}$ cells transiently express $Nur77^{GFP}$ when they are stimulated by Ag recognition (Au-Yeung et al., 2014; Bautista et al., 2016; Moran et al., 2011). Naïve OT-II.$Nur77^{GFP}$.Thy1.1^{+} CD4 T cells were transferred into wild-type (WT) hosts infected with PR8-OVA_{II}. NKG2A/C/E expression, identifying donor ThCTL in the lung (Marshall et al., 2016), was higher in the $Nur77^{GFP+}$ subset at 6 dpi compared to the $Nur77^{GFP-}$ subset (Fig S1A), indicating they have recently recognized Ag.

We used the sequential transfer approach (Bautista et al., 2016) to determine if 6 dpi effectors require Ag to become ThCTL (Figure 1A). We transferred naïve OT-II cells into hosts that were then infected with PR8-OVA_{II} (1st hosts). We isolated *in vivo*-generated OT-II effectors at 6 dpi. These were transferred into 2nd hosts that had been infected 6d previously (infection-matched). The 2nd hosts provided either Ag and infection (PR8-OVA_{II} infection), infection without Ag (PR8 infection) or neither (uninfected) (Figure 1A). Donor ThCTL generation was assessed 2 days post transfer (dpt) in the lung which corresponded to 8 days post infection. Donor ThCTL developed when Ag was presented in the 2nd hosts as expected (positive control), but their number was drastically reduced when Ag was absent (7x) (Figure 1B). The Ag-dependence was selective for ThCTL, as the total number of donor lung effectors was only reduced 1.7x (Fig S2A). Donor expression of indicators of cytotoxicity, that also characterize ThCTL, such as Granzyme B (GzmB) (Figure 1C) and the degranulation marker CD107a (Figure 1D), also depended on Ag presented in the 2nd host. Expression of other ThCTL-associated markers (Marshall et al., 2016)

by the donor lung effectors: PD1, CXCR6 and SLAM, were also Ag dependent, but active PSGL1 and CXCR3 were not (Figure S2B-F).

To assess *in vivo* cytotoxic function, the *in vivo*-generated effectors were transferred into 2nd hosts with or without Ag (as in Figure 1A) and additionally with CFSE-labeled target cells (Figure 1E). We found over 20% cytotoxicity (Ag-specific) in PR8-OVA$_{II}$-infected hosts, but little cytotoxicity in PR8-infected hosts. Thus, donor cell mediated CD4 cytotoxicity only developed when effectors were exposed to Ag, correlating with percentage and number of ThCTL in Figure 1B.

We also analyzed secretion of canonical Th1 effector cytokines such as IFNγ and TNFα by donor cells. In contrast to ThCTL that depend on Ag, the donor effectors recovered did not require Ag recognition to maintain the ability to secrete IFNγ and in fact TNFα secretion was lost when cognate Ag was present during the effector checkpoint (Figure 1F-G, Figure S2G). Thus, a program leading to induction of ThCTL phenotypes and functions, but not general Th1 characteristics, were coordinately driven in 6d effectors by cognate Ag recognition.

Cognate Ag recognition at the effector checkpoint drives generation of T$_{FH}$, GC-T$_{FH}$ and GCB in spleen and DLN

T$_{FH}$, like ThCTL, peak at 7-8 dpi (Figure S1D) and express specialized tissue-restricted and functional programs (Fazilleau et al., 2009; Lee et al., 2015; Vinuesa et al., 2016). In the same experiment as in Figure S1A, T$_{FH}$ (CXCR5^{hi}Bcl6^{hi}) were also enriched in the Nur77^{GFP+} population at 6 dpi in both the lung draining lymph nodes (DLN) and the spleen, indicating they had recently recognized Ag (Figure S1B-C). To test if 6d effectors require cognate Ag recognition to fully develop into T$_{FH}$ in the secondary lymphoid organs (SLO), we assessed T$_{FH}$ and more differentiated germinal center T$_{FH}$ (GC-T$_{FH}$) using the sequential transfer system described in Figure 1A. In the PR8-OVA$_{II}$ infection-matched positive controls, a strong donor T$_{FH}$ response

developed, while in PR8 infected-matched hosts without cognate Ag, very few donor T_{FH} were found in either the spleen (Figure 2A) or the DLN (Figure S3B).

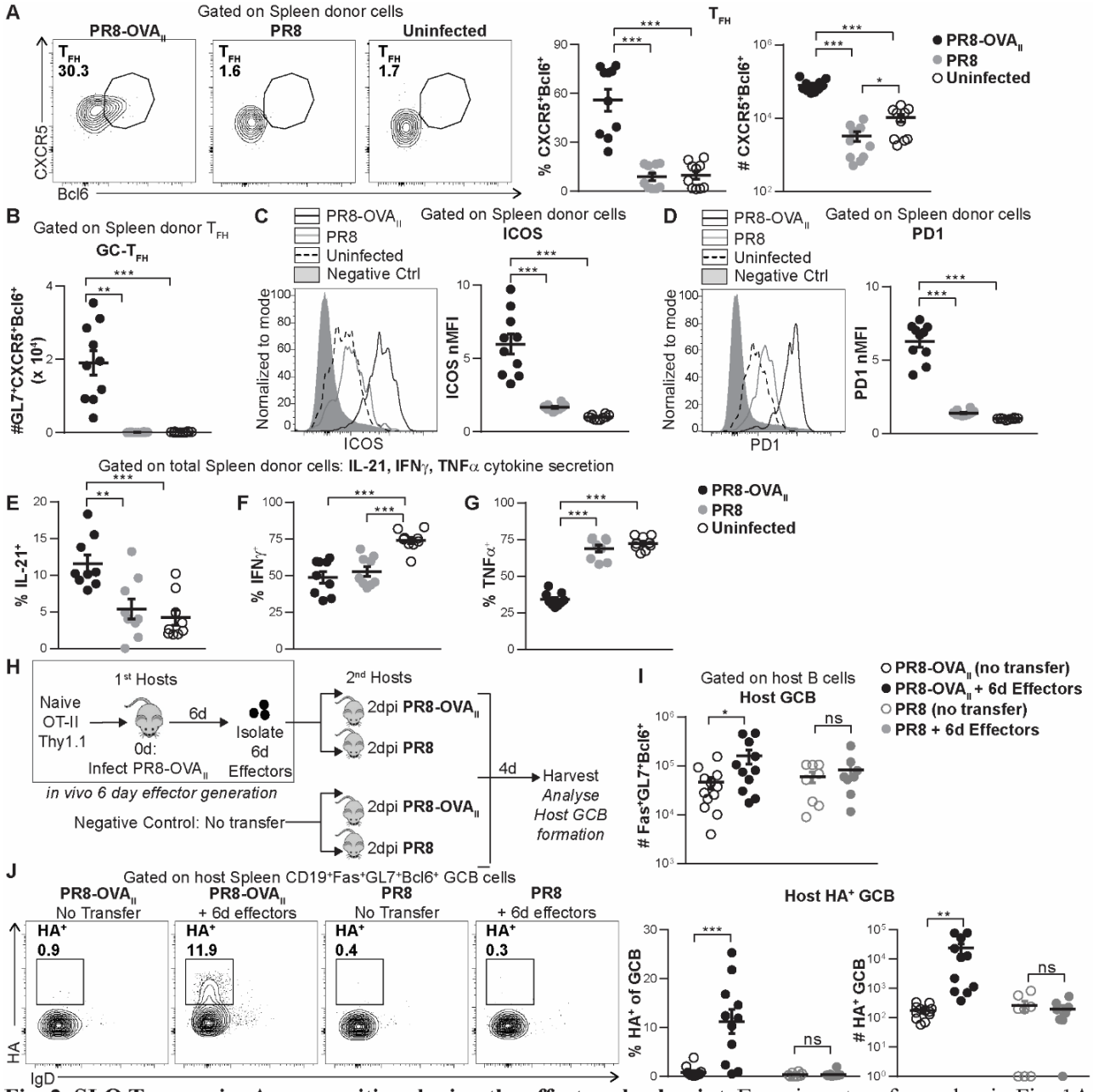

Fig. 2. SLO T_{FH} require Ag recognition during the effector checkpoint. Experiment performed as in Fig. 1A for Fig. 2A-G. **(A)** Percentage and numbers of spleen donor T_{FH} ($CXCR5^+Bcl6^+$). **(B)** Number of spleen donor germinal center T_{FH} ($GL7^+CXCR5^+Bcl6^+$). **(C-D)** Representative histogram of ICOS (C) and PD1 (D) expression by spleen donor cells (negative control: naïve CD4 from uninfected mice). Normalized ICOS MFI (C) and PD1 MFI (D) expression by spleen donor cells. (A-D, n= 10 per group pooled, 2 independent experiments). **(E-G)** Percentage of spleen donor cells expressing intracellular IL-21 (E), IFNγ (F) and TNFα (G) (n= 9 per group pooled, 2 independent experiments). **(H)** Experimental design for (I-J): *In vivo* generated 6d OT-II.Thy1.1$^+$ effectors were transferred into 2 dpi PR8-OVA_{II}-infected or PR8-infected mice. A group of 2 dpi PR8-OVA_{II}-infected and PR8-infected mice, with no cells transferred, served as negative controls. Spleens from these mice were analyzed 4 dpt. **(I)** Number of host GCB cells ($CD19^+Fas^+GL7^+Bcl6^+$) formed. **(J)** Percentage and numbers of HA^+ GCB. (H-I, n=8-12 per group pooled, 2-3 independent experiments). Error bars represent s.e.m. Statistical significance determined by two-tailed, unpaired Student's t-test (* $P < 0.05$, ** $P < 0.01$, *** $P < 0.001$). See also Fig. S3

Moreover, while they developed well in hosts with Ag, no donor GC-T_{FH} were generated without Ag (Figure 2B, Figure S3C-D). T_{FH}/GC-T_{FH}-associated molecules PD1 and ICOS were highly expressed by day 8 only when Ag was available (Figure 2C-D, Figure S3E-F), and were reduced in the absence of Ag. Thus, results from the same sequential transfer experiment (Figure 1A) showed that spleen and DLN T_{FH} (Figure 2A-D, Fig S3C-F), like lung ThCTL (Figure 1B-D), required cognate Ag recognition during the effector phase.

IL-21 promotes T_{FH} differentiation and is also produced by $T_{FH.}$ It mediates T_{FH} function during the GC response (Vinuesa et al., 2016). Indeed, the proportion of donor effectors secreting IL-21 was higher in 2nd hosts with Ag than in those without Ag (Figure 2E, Figure S3G). In contrast, the ability to maintain production of cytokines not directly associated with T_{FH}, such as IFNγ and TNFα were not Ag-dependent (Figure 2F-G). This indicates a selective dependence of T_{FH}-associated programs, but not other effector functions, on Ag recognition during the effector checkpoint.

To evaluate the impact of Ag recognition at the effector checkpoint, on T_{FH} function of helping GCB formation, we developed an *in vivo* GCB assay (Figure 2H). Endogenous host GCB are undetectable from 2-6 dpi after influenza infection (Figure S3H) because T_{FH} have not yet fully formed (Figure S1D). However, we reasoned that if functional T_{FH} were available earlier, they should accelerate GCB formation. Therefore, we transferred *in vivo* generated 6d OT-II effectors into hosts infected 2d previously with either PR8 (no cognate Ag) or PR8-OVA_{II} (cognate Ag available) and analyzed host GCB 4d after transfer (6 dpi). Thus, this model allowed us to study the acceleration of host GCB formation, during a timeframe (2-6 dpi) when their endogenous GCB formation was low. Transfer of 6d donor effectors into PR8-OVA_{II}-infected mice, caused a significant increase in total GCB formation (Figure 2I) and HA^+ GCB formation (Figure 2J) while

their transfer to PR8-infected hosts did not boost GCB formation over the negative controls which received no effectors. These results indicate that the critical T_{FH} function of inducing GCB cells and thus protective Ab responses, requires cognate Ag during the effector phase. Therefore, effector phase recognition of Ag is needed to drive induction of the key defining phenotypic and functional aspects of both ThCTL and T_{FH} programs, leading to their development in their respective niches.

T_{FH} but not ThCTL require CD28 co-stimulation at the effector checkpoint

T cells express CD28, which interacts with CD80/86 on APC during cognate interaction, co-stimulating IL-2 production and initiating proliferation (Watts, 2010). We analyzed whether ThCTL generation requires CD28:CD80/CD86 co-stimulation during the effector checkpoint. 6d *in vivo* effectors were transferred into WT or CD80/86 deficient PR8-OVA_{II} infection-matched hosts (Figure 3A). The recovery of total donor effectors in the lung was decreased (Figure S4A), when hosts lacked costimulatory ligands, but the proportion of lung donor ThCTL was increased (Figure 3B). Donor ThCTL numbers were unchanged (Figure 3B), suggesting non-ThCTL were lost, while ThCTL were retained. The level of NKG2A/C/E expression on donor ThCTL was increased in CD80/86KO compared with WT (Figure S4B) hosts, suggesting that the differentiation of ThCTL improved without CD28:CD80/86 co-stimulation. Next, we cultured *in vivo*-generated 6d effectors for 2d *in vitro* with anti-CD3 vs anti-CD3 plus CD28, to mimic effector phase Ag exposure, with and without CD28 co-stimulation (Figure 3C). No ThCTL developed without anti-CD3 (Figure S4C-D), mimicking the *in vivo* requirement for cognate Ag during the effector phase, as shown in Figure 1.

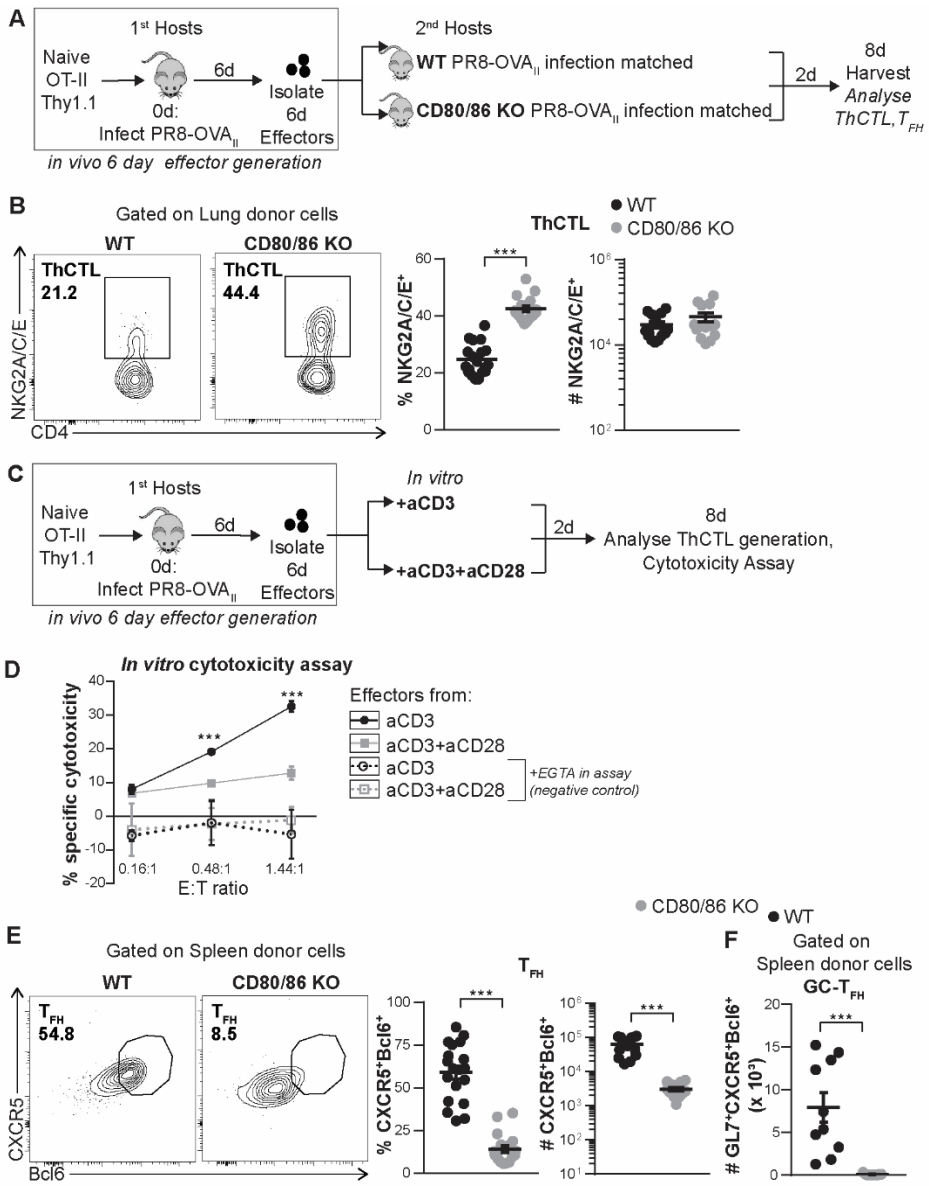

Fig. 3. T_{FH} and ThCTL have different effector phase CD28 co-stimulation requirements. (A) Experimental design for (B,E-F): *In vivo* generated 6d OT-II.Thy1.1^{+} effectors were transferred into 6 dpi PR8-OVA$_{II}$-infected WT or CD80/CD86$^{-/-}$ mice. Spleen, DLN and lungs were harvested at 8 dpi. **(B)** Percentage and number of lung donor ThCTL (NKG2A/C/E^{+}) (n=14-19 per group pooled, 4 independent experiments). **(C)** Experimental design: *In vivo* generated 6d OT-II.Thy1.1^{+} effectors were isolated and stimulated with either anti-CD3 alone or anti-CD3 and anti-CD28 *in vitro* to mimic *in vivo* effector phase cognate Ag stimulation. **(D)** Ag specific cytotoxicity of donors generated as in Fig. 3C, with anti-CD3 or anti-CD3 + anti-CD28 (Each E:T ratio is assayed in triplicate or single wells for +EGTA conditions, representative of 2 independent experiments). **(E-F)** Experiment done as in Fig. 3A. **(E)** Percentage and number of spleen donor T_{FH} (n=14-19 per group pooled, 3-4 independent experiments). **(F)** Number of spleen donor GC-T_{FH} (GL7^{+}CXCR5^{+} Bcl6^{+}) (n=8-10 per group pooled, 2 independent experiments). Error bars represent s.e.m. Statistical significance determined by two-tailed, unpaired Student's t-test (* P<0.05, ** P<0.01 and *** P<0.001). See also Fig. S4.

259

ThCTL developed when effectors were stimulated by CD3 alone and adding CD28 co-stimulation inhibited ThCTL generation (Figure S4D). Cytotoxic function also depended on anti-CD3 stimulation and was inhibited when CD28 co-stimulation was provided *in vitro* (Figure 3D). Together the *in vitro* and *in vivo* results indicate that ThCTL differentiation from 6d effectors does not require CD28 co-stimulation. The lack of a need for CD28 co-stimulation is also reminiscent of human ThCTL that studies have defined as CD28 negative populations (Serroukh et al., 2018; van de Berg et al., 2008).

In the same experiments (Figure 3A), both the proportion and absolute number of donor T_{FH} and GC-T_{FH} in the spleen and DLN were dramatically lower in the CD80/86 KO hosts (Figure 3E-F, Figure S4E-F). This agrees with previous data showing that CD28 co-stimulation post priming is necessary for T_{FH} generation and maintenance (Linterman et al., 2014). Thus, CD28 co-stimulation of CD4 effectors at the effector checkpoint is required for full development of T_{FH} in the spleen and the DLN but is not required to sustain or induce further ThCTL generation in the lung. This indicates that while both pathways of tissue-restricted effector development require Ag, the two have distinct co-stimulation requirements during the effector phase. This is consistent with a potential for multiple fate decisions taking place at this effector checkpoint, depending on the details of the cognate interactions.

Multiple APC subsets can effectively present Ag at the effector checkpoint to drive T_{FH} and ThCTL development

We wondered if the distinct CD28 co-stimulation requirements for ThCTL and T_{FH} subset development might reflect a requirement for distinct APC subsets. To evaluate the efficacy of different broad classes of APC at the effector checkpoint, we used MHC-II KO bone marrow

chimeras, CD11cTg.H2-Ab1$^{-/-}$ mice and JhD mice as 2nd hosts or provided Ag on distinct APC subsets (Figure 4A).

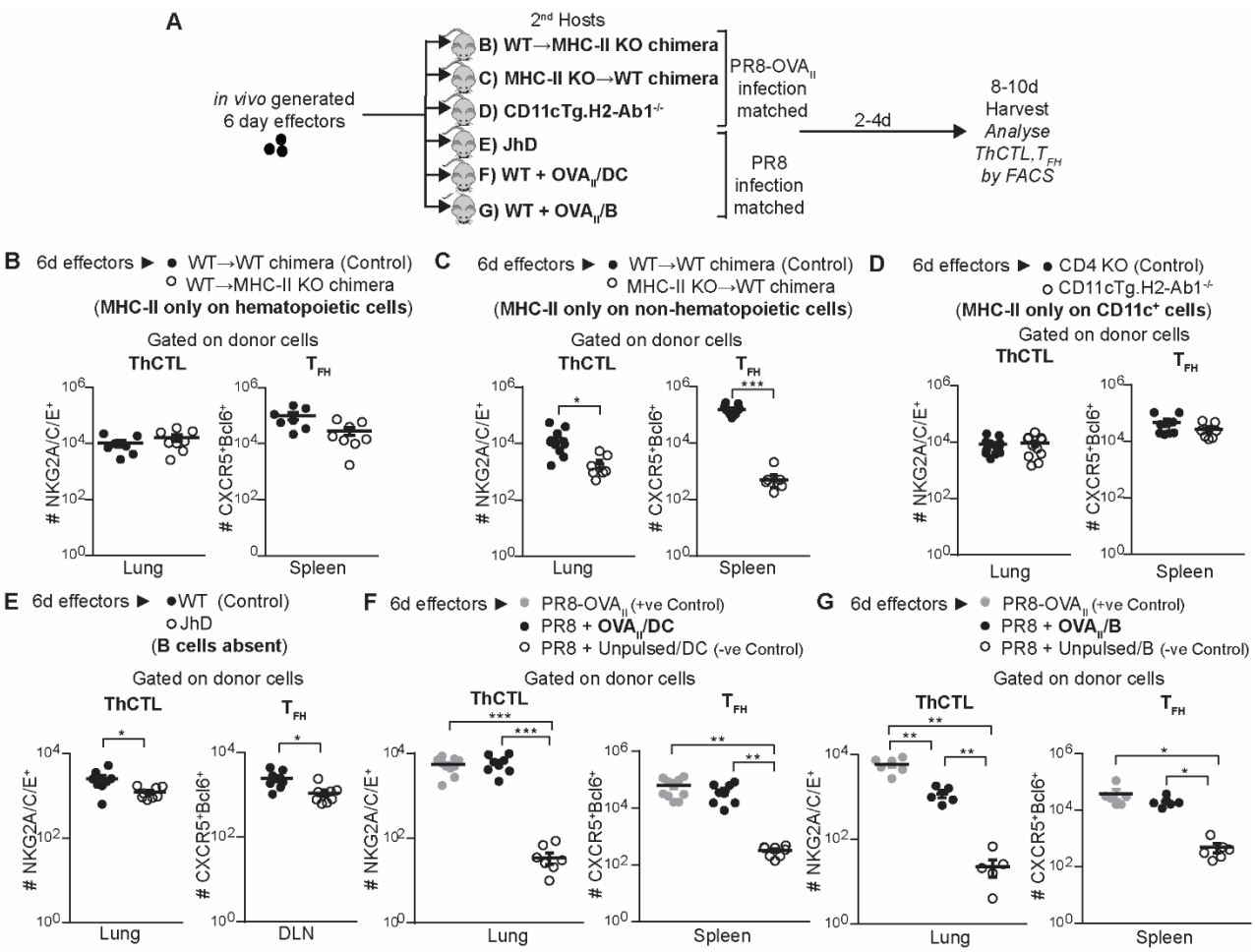

Fig. 4. Multiple APC subsets are able to present cognate Ag during the effector phase to support T_{FH} and ThCTL generation from 6d effectors. (A) Experimental design: *In vivo* generated 6d OT-II.Thy1.1^{+} or 6d HNT.Thy1.1^{+} effectors were transferred into PR8-OVA$_{II}$ infection-matched hosts (B-D), PR8 infection-matched hosts (E), or into PR8 infection-matched hosts together with OVA$_{II}$/APC (F-G). Numbers of T_{FH} (CXCR5^{+}Bcl6^{+}) and ThCTL (NKG2A/C/E^{+}) generated were enumerated by flow cytometry, 2-4 dpt in each of these models. **(B)** WT→ MHC-II KO (H2-Ab1$^{-/-}$) bone marrow chimera mice that were made by transferring WT bone-marrow into MHC-II KO irradiated hosts, where MHC-II is restricted to the hematopoietic compartment, or into WT→ WT bone marrow chimera control mice (n=7-8 per group pooled, 3 independent experiments). **(C)** MHC-II KO →B6 bone marrow chimera mice, where MHC-II is restricted to the non-hematopoietic compartment, or into WT→WT bone marrow chimera control mice (n=8-11 per group pooled, 3 independent experiments). **(D)** CD11cTg.H2-Ab1$^{-/-}$ mice where MHC-II is restricted to CD11c^{+} cells or into CD4 KO control mice (n=7-11 per group pooled, 2-3 independent experiments). **(E)** JhD mice where B cells are absent or into WT control mice (n=8 per group pooled, 2 independent experiments). **(F)** WT mice with cognate Ag supplied via OVA$_{II}$ pulsed BMDC vs unpulsed BMDC controls (n=8-10 per group pooled, 3 independent experiments). **(G)** WT mice with cognate Ag supplied via OVA$_{II}$ pulsed B cells vs unpulsed B cell controls (n=5-6 per group pooled, 2 independent experiments). Error bars represent s.e.m. Statistical significance determined by two-tailed, unpaired Student's t-test (* P<0.05, ** P<0.01 and *** P<0.001). See also Fig.S5.

We transferred 6d effectors into infection-matched BM chimeras in which MHC II Ag-presentation was restricted to either the hematopoietic compartment [WT → MHC-II KO chimeras] (Figure 4B, Figure S5A) or to the non-hematopoietic compartment [MHC-II KO→ WT chimeras] (Figure 4C, Figure S5B). There was no defect in ThCTL generation when MHC-II was restricted to the hematopoietic compartment. A substantial ThCTL population was also generated when MHC-II was restricted to non-hematopoietic cells though we found significantly fewer donor ThCTL (Figure 4C). Since a substantial ThCTL population was generated in both chimeras (Figure 4B-C, Figure S5A-B), it suggests that both hematopoietic and non-hematopoietic APC can present the Ag, to drive ThCTL development at the effector checkpoint. MHC-II is upregulated on infected epithelial cells in the lung during IAV infection, so they may be a source of non-hematopoietic APC (Brown et al., 2012). Donor T_{FH} were found when Ag was restricted to the hematopoietic compartment (Figure 4B, Figure S5A). In contrast, few if any T_{FH} were found when Ag presentation was restricted to the non-hematopoietic compartment (Figure 4C, Figure S5B), consistent with few non-hematopoietic MHC-II^{+} cells presenting Ag in the SLO (Malhotra et al., 2013).

Since the hematopoietic compartment was sufficient to support Ag presentation to both T_{FH} and ThCTL, we next asked if either of the classic APC: B cells and DCs, would be sufficient to drive the tissue-restricted effectors. We restricted Ag-presentation to CD11c^{+} APCs by using CD11cTg.H2-Ab1$^{-/-}$ mice (Figure 4D, Figure S5C). There was no defect in either donor ThCTL or T_{FH} formation when 6d effectors were transferred into PR8-OVA$_{II}$ infection-matched mice with MHC-II only on CD11c^{+} APC, indicating that CD11c^{+} APC are sufficient to drive both ThCTL and T_{FH} during the effector checkpoint.

B cells are the major APC for T_{FH} differentiation once they arrive in the follicular region of the SLO (Krishnaswamy et al., 2018). To test whether B cells were necessary as APC for driving tissue-restricted effectors during the effector checkpoint, we transferred *in vivo* generated 6d HNT Thy1.1 (TCR Tg specific for HA epitope of the influenza strain) effectors into PR8 infection-matched B cell deficient JhD mice (Figure 4E, Figure S5D). Substantial numbers of ThCTL and T_{FH} were generated in the B cell deficient JhD hosts, though in both cases there was a two-fold decrease in the number. This suggests that although B cell do contribute during the effector phase as APC, non-B cells can also serve as APC for both ThCTL and T_{FH} pathways.

We evaluated the impact of providing Ag on two different professional APC subsets: DC (Figure 4F, Figure S5E) and B cells (Figure 4G, Figure S5F). OVA_{II}/APC were transferred together with *in vivo* generated 6d effectors into PR8 infection-matched mice. The 6d effectors gave rise to ThCTL and T_{FH} when either B cells or DC presented Ag (Figure 4F-G, Figure S5E-F). We have established previously that the OVA_{II}/DC present Ag for less than 2d *in vivo* (Bautista et al., 2016). The OVA_{II}/DC transfer experiments suggest that, as for memory generation (Bautista et al., 2016), Ag recognition for the generation of T_{FH} and ThCTL, is only required for less than 2d after effector transfer, indicating a short window for Ag recognition and a temporally-defined checkpoint.

Thus, multiple subsets of APC efficiently presented Ag to effectors to drive ThCTL formation including activated professional APC, such as DC and B cells, as well as non-hematopoietic cells in infected mice. T_{FH} were generated in all experiments where hematopoietic MHC-II^+ presentation was available to the 6d effectors during the effector checkpoint. Thus, development of both CD4 tissue effectors during the effector phase, is independent of any unique APC type, with multiple APC able to be drive these fates.

Ag delivery to the lung during the effector phase selectively drives lung ThCTL generation

We hypothesized that Ag recognition during the effector checkpoint might be required in the site of residence to drive tissue-restricted effectors and that this might act to establish residency. To evaluate this for ThCTL generation, we first tested whether intranasal (i.n.) delivery of Ag/APC could target Ag presentation to the lung. We also transferred Ag/APC intrasplenically (i.s.) to exclude Ag presentation in the lung.

	APC localization			Nur77^{GFP} expression by OT-II Where are the OT-II that just saw Ag?		
	i.n.	i.v.	i.s.	i.n.	i.v.	i.s.
Spleen	✗	✓	✓	✗	✓	✓
DLN				✓	✓	✗
Lung	✓	✗	✗	✓	✓	✗

Table 1. Distribution of APC and Ag presentation in different sites using intranasal (i.n.), intravenous (i.v.) or intrasplenic (i.s.) transfer of APC. Data summarized from Fig 5B-C, 5F-G, 6A, 6E

We evaluated the localization of the APC using i.n. and i.s. delivery, and also evaluated corresponding Ag recognition by the transferred OT-II in the different sites (Table 1). To evaluate Ag recognition by effectors in the different sites using Nur77^{GFP} expression, we transferred OT-II.Nur77^{GFP}.Thy1.1^{+} 6d effectors into PR8 infection-matched hosts with the OVA$_{II}$/APC and analyzed them 14-16hr post transfer (Figure 5A). Only i.n. transfer of OVA$_{II}$/APC induced Nur77^{GFP} expression in donor effectors in the lung while i.s. transfer did not induce Nur77^{GFP} expression over the negative control where APC without Ag (unpulsed APC) were transferred (Figure 5B). In concert with the site of Ag recognition as seen with Nur77^{GFP} expression, OVA$_{II}$/APC were found only in the lung with i.n. transfer and only in the spleen with i.s. transfer (Figure 5C). These results indicate that we achieved localization of APC and successfully restricted Ag presentation to the lung with i.n. transfer of Ag/APC and that i.s. transfer of Ag/APC serves as a control where Ag is not presented locally in the lung (Table 1).

We then analyzed ThCTL generation from the 6d effectors, 3 days after transfer, at 9 dpi. Both i.n. and i.s. Ag/APC transfer increased trafficking of total transferred effectors to the lung, compared to the negative control (Figure 5D). We compared ThCTL generation after i.n. vs i.s. Ag/APC delivery (Figure 5E). Strikingly, only i.n. delivery induced ThCTL. When we used i.s. delivery, few if any ThCTL were generated, suggesting that Ag in the lung is required for lung ThCTL generation.

To test if peripheral Ag was sufficient to drive 6d effectors to ThCTL, we transferred OVA_{II}/APC i.v. and compared ThCTL generation to i.n. OVA_{II}/APC transfer. OT-II.Nur77^{GFP}.Thy1.1^{+} 6d effectors were also transferred into PR8 infection matched hosts (Figure 5A). 14-16hr after transfer, donor effectors in the lung expressed Nur77^{GFP} when OVA_{II}/APC were transferred either i.v. or i.n., indicating Ag recognition (Figure 5F). A greater proportion of donor effectors in the lung expressed Nur77^{GFP} in hosts that received i.v. OVA_{II}/APC compared to those that received i.n. OVA_{II}/APC. However, transferred APC were found predominantly in the spleen with many fewer in the lung with i.v. APC transfer (Figure 5G). This is compatible with the hypothesis that after i.v. OVA_{II}/APC transfer, donor effectors initially recognize Ag in the periphery before migrating to the lung (Table 1).

OVA_{II}/APC transfer i.v., like i.s., increased trafficking of transferred effectors to the lung, compared to the negative control and even compared to i.n. OVA_{II}/APC transfer (Figure 5H). These data (Figure 5D, Figure 5H) support the concept, that Ag presentation in the spleen enhances pathways that favor migration of T cells to the lung.

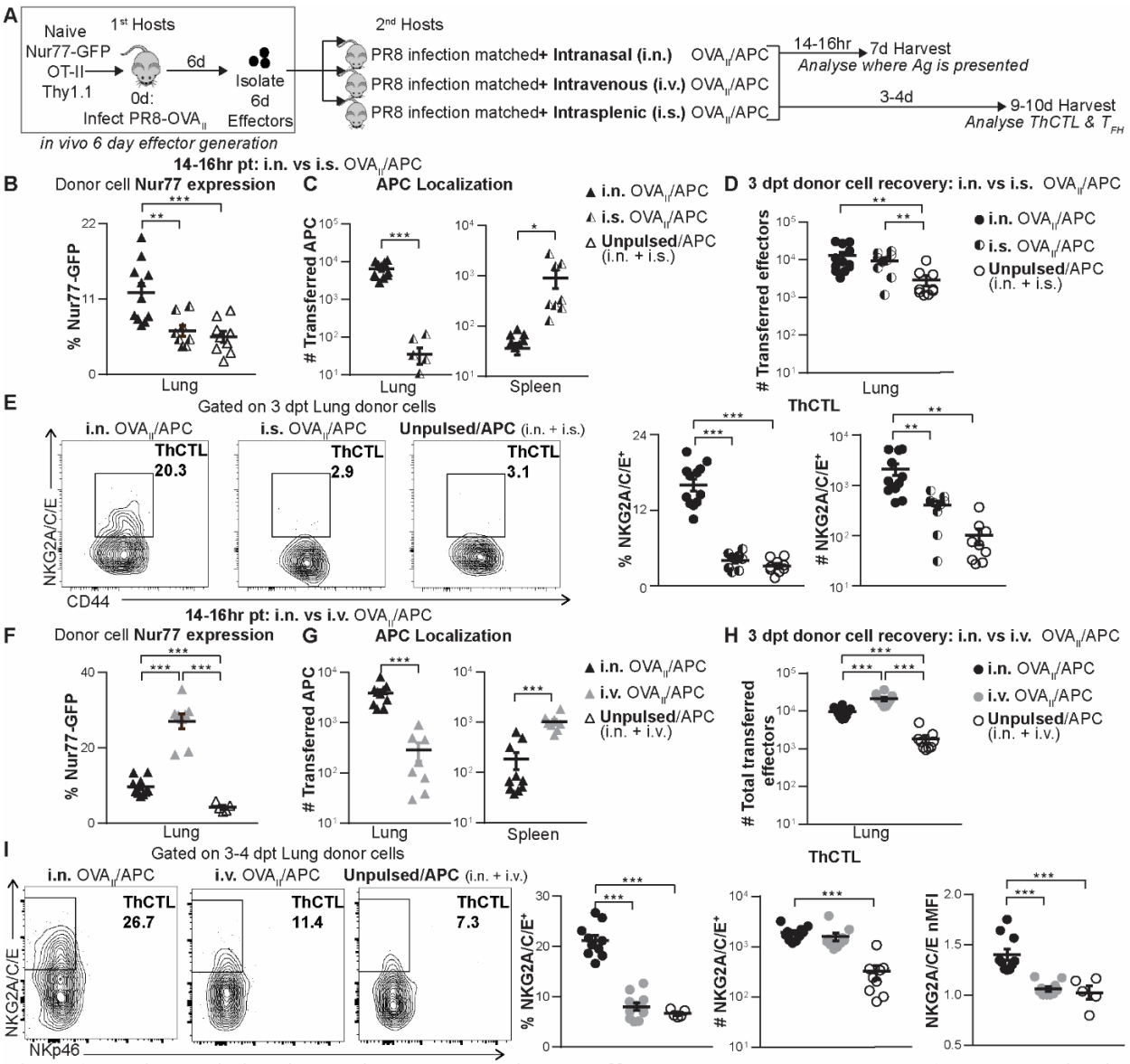

Fig. 5. Ag delivery via i.n., i.s and i.v. routes, during the effector phase, shows that local Ag presentation in the lung drives ThCTL generation from effectors. (A) Experimental design: OVA_{II} peptide pulsed B-cells ($CD45.1^+$ or GFP^+) were used as APC and transferred into PR8 infection-matched hosts 6 dpi either intranasally (i.n.), intrasplenically (i.s.) or intravenously (i.v.). Unpulsed APC were transferred both i.n. and i.s. (B-E) or i.n. and i.v. (F-I) as negative controls. *In vivo* generated 6d OT-II.$Nur77^{GFP}$.$Thy1.1^+$ effectors were transferred i.v. Mice were harvested 14-16hr post-transfer (pt) and donor cells were analyzed by flow cytometry. **(B)** Donor $Nur77^{GFP}$ expression (i.n. vs i.s. APC). **(C)** Number of transferred APC (i.n. vs i.s.) **(D-E)** Experiment performed as in (A) and mice harvested 3-4 dpt. **(D)** Number of donor effectors recovered with i.n. vs i.s. APC transfer. **(E)** Lung donor ThCTL formation with i.n. vs i.s. APC transfer. **(F-H)** Experiment performed as in (A). Mice harvested 14-16hr post-transfer (pt) **(F)** Donor $Nur77^{GFP}$ expression (i.n. vs i.v. APC) **(G)** Number of transferred APCs (i.n. vs i.v.). **(H-I)** Experiment performed as in (A). Mice were harvested 3-4 dpt. **(H)** Number of lung donor effectors with i.n. vs i.v. APC.**(I)** Donor lung ThCTL formation with i.n. vs i.v. APC. (B-C, F-G: n=8-11 per group pooled, 3 independent experiments. D-E, H-I: n=5-12 per group pooled, 2-4 independent experiments) Error bars represent s.e.m. Statistical significance determined by two-tailed, unpaired Student's t-test (* $P < 0.05$, ** $P < 0.01$ and *** $P < 0.001$). See also Fig S6.

389

Development of donor ThCTL in the lung as measured by NKG2A/C/E expression (both percent and MFI) after i.v. transfer, was as low as the negative control (Figure 5I). CXCR6 and PD1 expression by the NKG2A/C/E^{+} cells generated with i.v. OVA$_{II}$/APC transfer was also lower compared to those generated with i.n. OVA$_{II}$/APC (Figure S6A). This suggests that i.v. OVA$_{II}$/APC did not optimally support full ThCTL differentiation even if 6d effectors recognize Ag initially in the SLO, before migrating to their site of residence in the lung. Thus, we suggest that peripheral Ag enhances migration of effectors to the lung, but ThCTL develop optimally only when Ag is presented in the tissue of residency, the lung.

Delivery of Ag by different routes favors Ag presentation in distinct SLO during the effector phase and selectively drives DLN T$_{FH}$ or spleen T$_{FH}$

T$_{FH}$, like ThCTL, are restricted to the SLO (DLN and spleen) and express signatures for residency in SLO (Fazilleau et al., 2009; Lee et al., 2015). We asked if DLN and spleen T$_{FH}$ required Ag presentation in their organ of residence to drive their development during the effector phase. Using the same approach for evaluating local Ag requirements as for ThCTL in Figure 5, we delivered Ag via OVA$_{II}$/APC either i.n. or i.s. and transferred OT-II.Nur77^{GFP}.Thy1.1^{+} 6d effectors into PR8 infection-matched hosts (Table 1). Transfer of OVA$_{II}$/APC i.n. induced Nur77^{GFP} expression in the DLN and not in the spleen, while i.s. transfer induced Nur77^{GFP} exclusively in donor cells recovered from the spleen and not in the DLN (Figure 6A). These results indicate that we had successfully restricted Ag presentation using i.n. vs i.s. delivery to the either the DLN or the spleen respectively (Table 1).

We analyzed T$_{FH}$ generation from the 6d effectors, 3 days after transfer, at 9 dpi. The total number of donor cells recovered in the DLN, was increased following i.n. OVA$_{II}$/APC transfer but not with i.s. OVA$_{II}$/APC transfer and vice-versa for the number of donor cells recovered in the spleen

(Figure 6B). We found that T_{FH} in the DLN developed from the 6d effectors, only when OVA_{II}/APC were administered i.n. and not i.s. (Figure 6C). Conversely, spleen T_{FH} were supported only when OVA_{II}/APC were delivered i.s. and not when delivered i.n. (Figure 6D). Thus in the same experiment (Fig 5-6), T_{FH} like ThCTL, develop only when Ag is presented in the tissue of residency.

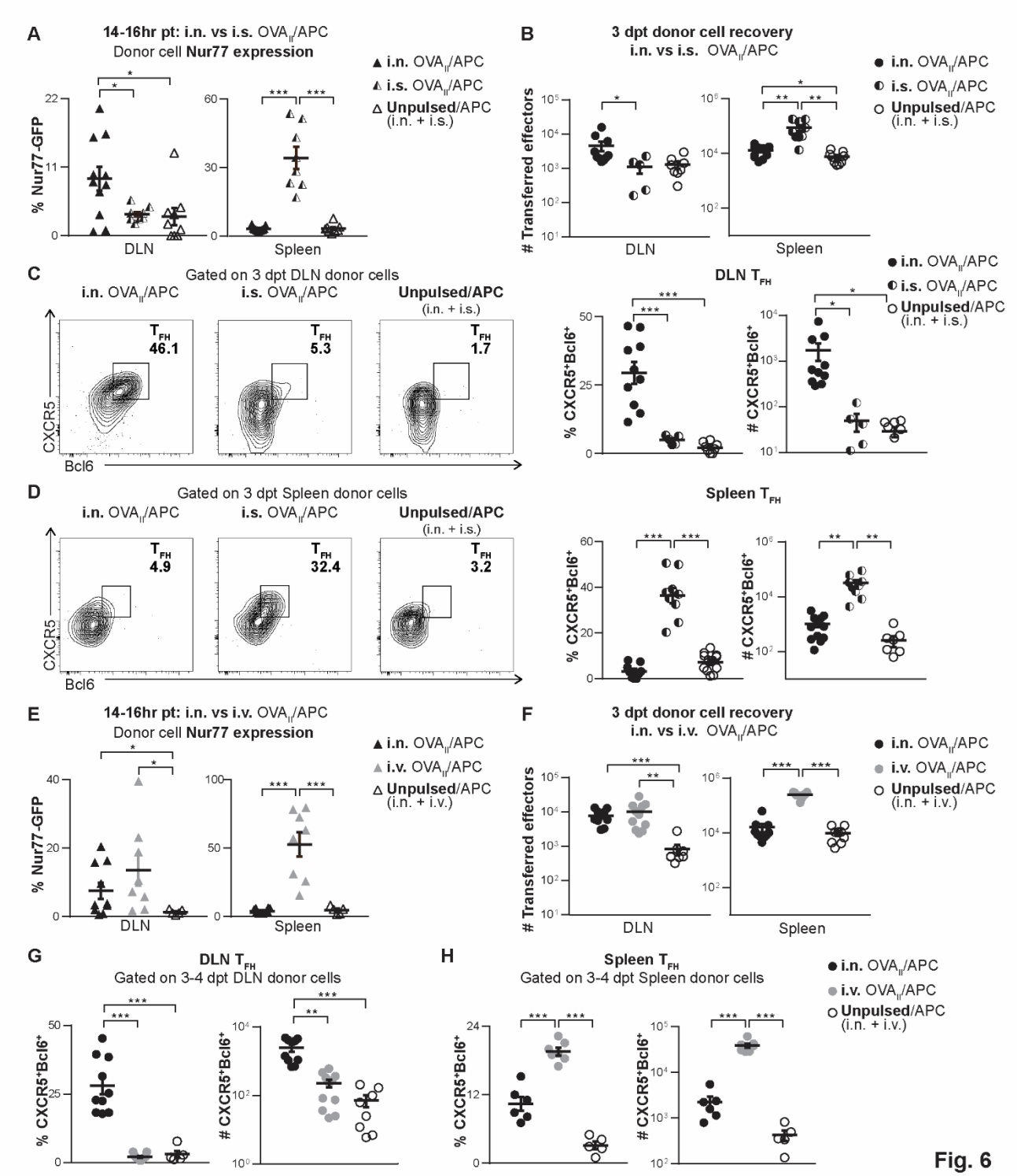

Fig. 6

Fig. 6. DLN T_{FH} and spleen T_{FH} require local Ag presentation during the effector phase as shown by Ag delivery via i.n., i.s and i.v. routes (A) Experiment was performed as in Fig. 5A. Mice were harvested 14-16hr post-transfer (pt) and donor cell Nur77^{GFP} expression was analyzed by flow cytometry in the DLN and spleen (i.n. vs i.s. APC). **(B-D)** Experiment was performed as in Fig. 5A and mice were harvested 3-4 dpt. **(B)** Total numbers of DLN and spleen donor effectors recovered with i.n. vs i.s. APC transfer (n=5-12 per group pooled, 3-4 independent experiments). **(C)** DLN donor T_{FH} formation with i.n. vs i.s. APC transfer (n=5-10 per group pooled, 3 independent experiments) **(D)** Spleen donor T_{FH} formation with i.n. vs i.s. APC transfer (n=9-12 per group pooled, 4 independent experiments). **(E)** Experiment was performed as in Fig. 5A. Mice were harvested 14-16hr post-transfer (pt) and donor cell Nur77^{GFP} expression was analyzed by flow cytometry in the DLN and spleen (i.n. vs i.v. APC). **(F-H)** Experiment was performed as in Fig. 5A. Mice were harvested 3-4 dpt. **(F)** Numbers of donor effectors in the DLN and spleen when APC were transferred i.n. vs i.v. (n=5-11 per group pooled, 2-3 independent experiments). **(G)** Donor T_{FH} formation in the DLN when APC were transferred i.n. vs i.v. (n=5-11 per group pooled, 2-3 independent experiments). **(H)** Donor T_{FH} formation in the spleen when APC were transferred i.n. vs i.v. (n=5-11 per group pooled, 2-3 independent experiments). Error bars represent s.e.m. Statistical significance determined by two-tailed, unpaired Student's t-test (* $P < 0.05$, ** $P < 0.01$ and *** $P < 0.001$). See also Fig. S6.

We also tested if peripheral Ag was sufficient to drive 6 dpi effectors to T_{FH} in the SLO. To do this, we transferred OVA_{II}/APC i.v. with OT-II.Nur77^{GFP}.Thy1.1^{+} 6d effectors. After 14-16hr, donor effectors in both the spleen and DLN expressed Nur77^{GFP}, indicating Ag recognition (Figure 6E, Table 1) though APC were found predominantly in the spleen with i.v. APC transfer (Figure 5G, Table 1). As seen for lung ThCTL, OVA_{II}/APC transferred i.v. did not support donor DLN T_{FH} generation but did support spleen T_{FH} (Figure 6G-H, Figure S6B-C). This suggests that even if 6d effectors recognize Ag initially before migrating to their site of residence in the DLN, this is insufficient to induce development of DLN T_{FH}.

Altogether, these results support the concept that the final steps in full-fledged tissue-restricted ThCTL and T_{FH} tissue-restricted effector generation from 6d effectors, require local Ag recognition in the site of residency.

DISCUSSION

While the instrumental role of Ag during the priming of T cells is well appreciated, we show here that signals from local Ag and co-stimulation, during the effector phase, are required to drive development of specialized T_{FH} and ThCTL tissue-restricted effectors. These results indicate that generation of these tissue-restricted effectors following influenza infection, unlike circulating Th1 effectors, require that infection continues into the effector phase to supply these Ag signals. Thus, if infection is absent at this checkpoint, few of these specialized tissue effectors will develop. Given the well-studied roles of ThCTL in viral clearance and T_{FH} in subsequent B cell Ab responses (Crotty, 2019; Juno et al., 2017; Marshall and Swain, 2011; McKinstry et al., 2012), the lack of these subsets will undermine a successful response. We postulate this checkpoint mechanism acts as a safeguard to limit T_{FH} and ThCTL generation to those situations where there is an ongoing threat, thereby limiting unnecessary, potentially harmful responses. Indeed, exaggerated ThCTL and T_{FH} responses are seen in certain autoimmune diseases and chronic infections (Broadley et al., 2017; Gensous et al., 2018) where continuous Ag and inflammation persist.

Requirements for repeated/prolonged Ag for generation of T_{FH} have been previously reported (Krishnaswamy et al., 2018), but this has been unexplored for other tissue-restricted CD4 effector subsets, such as ThCTL. It is known that T_{FH} require repeated Ag recognition and costimulatory interactions during priming and at the T-B border and in the GC of the SLO (Krishnaswamy et al., 2018). Thus, it is expected though unknown if T_{FH} will require Ag recognition, well into the late effector phase as well. We show that this is indeed the case, but also show that the requirement of CD4 effectors for Ag recognition at the checkpoint is not restricted to T_{FH} but part of a broader paradigm that drives multiple specialized CD4 responses, including T_{FH}, ThCTL and CD4

memory. Importantly, we find that the cognate Ag requirement during the effector phase for both ThCTL and T_{FH} can occur independently of both B cells and germinal centers. In addition, we show that CD4 effectors must recognize Ag in their tissue of residence to become tissue-restricted effectors.

ThCTL are not found until after 6 dpi (Marshall et al., 2016) and the 6d effectors we transfer express no ThCTL markers (Figure S1E). Thus, we interpret their dependence on effector phase cognate-Ag recognition, as driving their generation from CD4 effectors. On the other hand, the T_{FH} developmental program begins early during CD4 effector activation when effectors begin to express Bcl6 within the first few rounds of cell division (Vinuesa et al., 2016). Thus, the 6d effectors we transfer include some "pre-T_{FH}" at 6 dpi (Figure S1D). The 6d pre-T_{FH} have the potential to become T_{FH}, but our data here (25-fold reduction to negligible T_{FH} levels in the absence of Ag), suggest they only realize that potential if they receive signals from Ag recognition again, locally, during the effector phase. We plan further studies to explore which of the programs – differentiation/generation, expansion, survival/maintenance - are induced by Ag recognition in this model. Altogether, what is evident from our functional data is that, in the absence of Ag presentation during the effector phase, there are few if any T_{FH} that drive GC responses (Figure 2H-J) and few ThCTL that mediate MHC-II cytotoxicity (Figure 1E).

During polyclonal responses, new naïve CD4 T cells are recruited throughout the response (Jelley-Gibbs et al., 2005) and individual polyclonal cells have different propensities to become T_{FH} because of their different TCRs (Krishnaswamy et al., 2018).These features create a non-synchronized effector population which makes it difficult to identify cells at the same state of differentiation and track their fate. We circumvented these issues by generating effectors *in situ* from homogenous naïve TCR Tg CD4 T cells from two different models that gave corresponding

results: B6.OT-II and BALB/c.HNT. Moreover, we have reproduced the strict requirement for Ag recognition by CD4 effectors for memory generation in a BALB/c D0.11.10 model, in this B6.OT-II model (Bautista et al., 2016; McKinstry et al., 2014) and in a new influenza NP-specific TcR Tg. Usage of the TCR Tg sequential transfer model allowed the study of effector phase signals specifically, after 6 days post infection, which we could not have achieved using a polyclonal system.

Our experiments here focus solely on the requirements at the effector phase from 6 dpi onwards, coincident with the previously defined checkpoint for effectors in memory studies (Bautista et al., 2016; McKinstry et al., 2014). We identified several signals required to drive effectors at the checkpoint to T_{FH} and ThCTL. First, effectors became T_{FH} and ThCTL only when they recognized cognate Ag/APC at 6-8 dpi (Figure 1-2). Previously, we showed that CD4 memory generation required cognate Ag recognition 6-8 dpi and that this was dependent on autocrine IL-2 induction (Bautista et al., 2016; McKinstry et al., 2014). We confirmed the timeframe by blocking costimulatory pathways, blocking the IL-2 pathway and by adding back IL-2. The checkpoint coincides *in situ* with the peak of the effector response, which is followed by rapid contraction, supporting the concept that effectors express a default program of apoptosis which they avoid only when they recognize Ag (Bautista et al., 2016; McKinstry et al., 2014). We showed that the absence of effector checkpoint Ag results in poor CD4 memory development, corresponding with loss in protection against lethal influenza infection (Bautista et al., 2016). Thus, the development of three functionally specialized CD4 subsets, T_{FH}, ThCTL and CD4 memory, each requires cognate Ag recognition during this effector checkpoint. In addition to TCR triggering by Ag, T_{FH} but interestingly not ThCTL, required CD80/86 on the APC indicating distinct pathways are required for these distinct tissue-restricted effector subsets (Figure 3).

Second, we showed various activated MHC-II$^+$ APC, including DC and B cells, drove donor effectors to develop into T_{FH} and ThCTL (Figure 4) consistent with previous studies of APC subsets required during initial priming of T_{FH} responses (Deenick et al., 2010; Deenick et al., 2011). In our experiments, *in vivo* transferred DC present Ag for less than 48hr (Bautista et al., 2016) indicating that effectors only need a brief period of TCR triggering. T_{FH} were generated from 6d effectors even when Ag was presented only by DC (Figure 4F, Figure S5E) and even in the absence of B cells and GC in JhD 2nd hosts (Figure 4E, Figure S5D). Thus, although B cells may be the major source of Ag for T_{FH} *in situ*, other MHC-II$^+$ APC are competent to drive T_{FH} development at the effector phase. Given the critical importance of T_{FH} to effective B cell immunity, this may allow development of strong T_{FH} responses even if germinal center responses are impaired or Ag-specific B cells are limited. For instance, this may be a useful strategy for the immune system to be able to drive GC-independent B cell responses which benefit from T_{FH} help, such as reactivation of previously generated memory B cells (Inoue et al., 2018).

Third, the highest proportion and most well-differentiated T_{FH} and ThCTL developed only when APC was delivered to the site of future residence (Figure 5-6). Recently, Ag presentation in tissues has been implicated in development of both T and B resident memory subsets (Allie et al., 2019; Khan et al., 2016; McMaster et al., 2018; Takamura et al., 2016). Our data suggest that local Ag presentation in the tissue site, establishes residency during the effector checkpoint. Previous studies have largely focused on tissue-resident T cell subsets in non-lymphoid tissues, however SLO also have distinct architecture and function (Lewis et al., 2019; Malhotra et al., 2013). Here we show that SLO-resident T_{FH} subsets also have unique local Ag presentation requirements during the effector checkpoint (Figure 6) that are distinct from lung resident ThCTL and suggests that tissue-restricted Ag presentation is required even if they encountered Ag before entering the

local tissue niche (Figure 6E-H). A subset of SLO T_{RM} has also been identified recently (Beura et al., 2018; Schenkel et al., 2014). Thus, our results here and those recent studies, solidify the previously underappreciated concept that SLO also harbor tissue resident T cell subsets with unique requirements for differentiation.

The functional activity of T_{FH} and ThCTL correlated well with the availability of the checkpoint signals. T_{FH} required Ag recognition to produce IL-21 (Figure 2E) and to induce GCB (Figure 2H-J). Likewise, the generation of ThCTL correlated with their cytotoxic function against target cells (Figure 1E). Tissue-restricted effector functions are critical to immunity (Devarajan et al., 2018). T_{FH} drive GCB formation which leads to B cell isotype class switching, generation of high affinity somatically mutated B cells, and generation of long-lived plasma cells and memory B cells (Crotty, 2019). T_{FH} are required for, and are a reliable indicator of, protective Ab after influenza vaccination (Koutsakos et al., 2019b). ThCTL reduce viral titers and are associated with better disease control in many viral infections (Juno et al., 2017; Muraro et al., 2017; Phetsouphanh et al., 2017) and tumor models (Melssen and Slingluff, 2017), especially those where class I is downregulated by viruses and tumor microenvironments where CD8 cytotoxic cells are ineffective. Tissue-restricted effectors are also likely the precursors of T_{RM} which are at the frontline of immune defense to re-infection.

These results are directly relevant to vaccine design. The most common Ab viral epitopes on the surface proteins shift frequently, constraining the ability of long-lived Ab produced by B cells, to remain fully protective. Thus, T cells are central to broad immunity to influenza and other RNA viruses that mutate because the they target core proteins of viruses that rarely change (Devarajan et al., 2016). Our results suggest that vaccine approaches need to deliver Ag to tissues, such as Flumist which delivers Ag to the lung, if they are to efficiently drive the tissue-restricted CD4 T

cell subsets and CD4 memory. Additionally, unformulated soluble Ag/adjuvants in vaccines have been shown to be rapidly cleared from the body (Moyer et al., 2016), which may explain the low efficacy of current influenza vaccines in generating durable CD4 T cell responses and indirectly strong long-term B cell immunity. Several formulation strategies have been proposed such as synthetic polymer formulations, microneedle skin patches and polymer sponges to extend the kinetics of Ag presentation in vaccines (Moyer et al., 2016). One recent strategy engineered enhanced Ag binding on alum, which allowed Ag presentation well into the effector phase (Moyer et al., 2020) and elicited superior humoral immunity. We predict that such strategies are likely to better support tissue effector formation.

Coupled with our earlier studies of memory generation (Bautista et al., 2016; McKinstry et al., 2014), our results here support a new paradigm in which a set of critical fate decisions occur at the CD4 effector checkpoint to coordinately support generation of multiple alternate fates: CD4 memory, T_{FH} and ThCTL. We believe that the regulation of the response at the effector checkpoint by cognate Ag, can lend new perspective on mechanisms of autoimmune pathogenesis driven by CD4 tissue effectors. We also suggest that to induce durable immunity, the most effective vaccines must provide the effector checkpoint signals identified here at the right time and in the relevant sites, so as to drive robust tissue-restricted effector as well as memory cell generation resulting in both more effective immunity and more “universal” influenza protection (Devarajan et al., 2016).

ACKOWLEDGEMENTS

We would like to thank Dr. Richard Dutton, Dr. Kai McKinstry, Dr. Tara Strutt and Dr. Esteban Rozen for useful discussions and advice throughout the project. We would also like to thank Yi Kuang, Jialing Liang and Mike Perkins for assistance with experiments and animal husbandry. This work was supported by funding from grants U19 AI109858, P01 AI046530, R01 AI118820 and R21 AI128606 to S.L.S; T32 AI007349 to A.M.V., M.C.J. and O.K.U.; R25 GM113686 and T32 AI132152 to O.K.U.

AUTHOR CONTRIBUTIONS

P.D. and S.L.S. wrote the manuscript with assistance from A.M.V., B.L.B., M.C.J. and O.K.U. P.D., A.M.V. and S.L.S. conceived the project and designed experiments. P.D. and A.M.V. performed and analyzed experiments with assistance from C.H.C., B.L.B., M.C.J. and O.K.U. A.M.V. primarily performed and analyzed experiments for Figures 1-3 and associated supplementary figures. P.D. primarily performed and analyzed experiments for Figure 2, Figures 4-6 and associated supplementary figures. K.A.K. performed intrasplenic transfers with assistance from P.D. All authors have read and approved the submitted version.

DECLARATION OF INTERESTS

The authors declare no financial conflicts of interest.

FIGURE LEGENDS

Figure 1. Cognate Ag during the effector checkpoint is required for lung ThCTL phenotype and function. (A) Experimental design for (B-D): Naïve OT-II.Thy1.1^{+} cells were transferred into PR8-OVA$_{II}$ infected mice (1st hosts). At 6 dpi, OT-II.Thy1.1^{+} effectors were isolated from 1st hosts and transferred into following groups of 2nd hosts: 6 dpi PR8-OVA$_{II}$-infected, 6 dpi PR8-infected, or uninfected mice. Donor cells were analyzed 8 dpi. **(B)** Percentage and numbers of donor lung ThCTL (NKG2A/C/E^{+}) (n=19 per group pooled, 4 independent experiments). **(C)** Representative histogram of lung donor cell GzmB expression (negative control: naïve CD4 from uninfected mice). Normalized MFI of lung donor cell GzmB expression (n=10 per group pooled, 2 independent experiments). **(D)** CD107a degranulation marker expression by lung donor cells (n=9 per group pooled, 2 independent experiments). **(E)** Experimental design: *In vivo* 6d OT-II.Thy1.1^{+} effectors were transferred into 6 dpi PR8-OVA$_{II}$ or PR8 infection-matched TCRα/β$^{-/-}$ mice. CFSE^{lo} target and bystander CFSE^{hi} bystander cells were transferred at 7d. Representative CFSE histograms shown. Percentage Ag specific cytotoxicity in each group is shown. **(F-G)** Experiment done as in (E). Percentage of lung donor cells expressing intracellular IFNγ (F) and TNFα (G) (E-G, n=7 per group pooled, 2 independent experiments). Statistical significance determined by two-tailed, unpaired Student's t-test (* P<0.05, ** P<0.01, *** P<0.001). See also Figure S2.

Figure 2. SLO T$_{FH}$ require Ag recognition during the effector checkpoint. Experiment performed as in Figure 1A for Figure 2A-G. **(A)** Percentage and numbers of spleen donor T$_{FH}$ (CXCR5^{+}Bcl6^{+}). **(B)** Number of spleen donor germinal center T$_{FH}$ (GL7^{+}CXCR5^{+}Bcl6^{+}). **(C-D)** Representative histogram of ICOS (C) and PD1 (D) expression by spleen donor cells (negative control: naïve CD4 from uninfected mice). Normalized ICOS MFI (C) and PD1 MFI (D) expression by spleen donor cells. (A-D, n= 10 per group pooled, 2 independent experiments). **(E-**

G) Percentage of spleen donor cells expressing intracellular IL-21 (E), IFNg (F) and TNFa (G) (n= 9 per group pooled, 2 independent experiments). **(H)** Experimental design for (I-J): *In vivo* generated 6d OT-II.Thy1.1^{+} effectors were transferred into 2 dpi PR8-OVA$_{II}$-infected or PR8-infected mice. A group of 2 dpi PR8-OVA$_{II}$-infected and PR8-infected mice, with no cells transferred, served as negative controls. Spleens from these mice were analyzed 4 dpt. **(I)** Number of host GCB cells (CD19^{+}Fas^{+}GL7^{+}Bcl6^{+}) formed. **(J)** Percentage and numbers of HA^{+} GCB. (H-I, n=8-12 per group pooled, 2-3 independent experiments). Error bars represent s.e.m. Statistical significance determined by two-tailed, unpaired Student's t-test (* P<0.05, ** P<0.01, *** P<0.001). See also Figure S3.

Figure 3. T$_{FH}$ and ThCTL have different effector phase CD28 co-stimulation requirements. **(A)** Experimental design for (B, E-F): *In vivo* generated 6d OT-II.Thy1.1^{+} effectors were transferred into 6 dpi PR8-OVA$_{II}$-infected WT or CD80/CD86$^{-/-}$ mice. Spleen, DLN and lungs were harvested at 8 dpi. **(B)** Percentage and number of lung donor ThCTL (NKG2A/C/E^{+}) (n=14-19 per group pooled, 4 independent experiments). **(C)** Experimental design: *In vivo* generated 6d OT-II.Thy1.1^{+} effectors were isolated and stimulated with either anti-CD3 alone or anti-CD3 and anti-CD28 *in vitro* to mimic *in vivo* effector phase cognate Ag stimulation. **(D)** Ag specific cytotoxicity of donors generated as in Figure 3C, with anti-CD3 or anti-CD3 + anti-CD28 (Each E:T ratio is assayed in triplicate or single wells for +EGTA conditions, representative of 2 independent experiments). **(E-F)** Experiment done as in Figure 3A. **(E)** Percentage and number of spleen donor T$_{FH}$ (n=14-19 per group pooled, 3-4 independent experiments). **(F)** Number of spleen donor GC-T$_{FH}$ (GL7^{+}CXCR5^{+} Bcl6^{+}) (n=8-10 per group pooled, 2 independent experiments). Error bars represent s.e.m. Statistical significance determined by two-tailed, unpaired Student's t-test (* P<0.05, ** P<0.01 and *** P<0.001). See also Figure S4.

Figure 4. Multiple APC subsets are able to present cognate Ag during the effector phase to support T_{FH} and ThCTL generation from 6d effectors. (A) Experimental design: *In vivo* generated 6d OT-II.Thy1.1^{+} or 6d HNT.Thy1.1^{+} effectors were transferred into PR8-OVA_{II} infection-matched hosts (B-D), PR8 infection-matched hosts (E), or into PR8 infection-matched hosts together with OVA_{II}/APC (F-G). Numbers of T_{FH} (CXCR5^{+}Bcl6^{+}) and ThCTL (NKG2A/C/E^{+}) generated were enumerated by flow cytometry, 2-4 dpt in each of these models. **(B)** WT→ MHC-II KO (H2-Ab1$^{-/-}$) bone marrow chimera mice that were made by transferring WT bone-marrow into MHC-II KO irradiated hosts, where MHC-II is restricted to the hematopoietic compartment, or into WT→WT bone marrow chimera control mice (n=7-8 per group pooled, 3 independent experiments). **(C)** MHC-II KO →B6 bone marrow chimera mice, where MHC-II is restricted to the non-hematopoietic compartment, or into WT→WT bone marrow chimera control mice (n=8-11 per group pooled, 3 independent experiments). **(D)** CD11cTg.H2-Ab1$^{-/-}$ mice where MHC-II is restricted to CD11c^{+} cells or into CD4 KO control mice (n=7-11 per group pooled, 2-3 independent experiments). **(E)** JhD mice where B cells are absent or into WT control mice (n=8 per group pooled, 2 independent experiments). **(F)** WT mice with cognate Ag supplied via OVA_{II} pulsed BMDC vs unpulsed BMDC controls (n=8-10 per group pooled, 3 independent experiments). **(G)** WT mice with cognate Ag supplied via OVA_{II} pulsed B cells vs unpulsed B cell controls (n=5-6 per group pooled 2 independent experiments). Error bars represent s.e.m. Statistical significance determined by two-tailed, unpaired Student's t-test (* $P<0.05$, ** $P<0.01$ and *** $P<0.001$). See also Figure S5.

Figure 5. Ag delivery via i.n., i.s and i.v. routes, during the effector phase, shows that local Ag presentation in the lung drives ThCTL generation from effectors. (A) Experimental design: OVA_{II} peptide pulsed B-cells (CD45.1^{+} or GFP^{+}) were used as APC and transferred into PR8

infection-matched hosts 6 dpi either intranasally (i.n.), intrasplenically (i.s.) or intravenously (i.v.). Unpulsed APC were transferred both i.n. and i.s. (B-E) or i.n. and i.v. (F-I) as negative controls. *In vivo* generated 6d OT-II.Nur77^{GFP}.Thy1.1^{+} effectors were transferred i.v. Mice were harvested 14-16hr post-transfer (pt) and donor cells were analyzed by flow cytometry. **(B)** Donor Nur77^{GFP} expression (i.n. vs i.s. APC). **(C)** Number of transferred APC (i.n. vs i.s.) **(D-E)** Experiment performed as in (A) and mice harvested 3-4 dpt. **(D)** Number of donor effectors recovered with i.n. vs i.s. APC transfer. **(E)** Lung donor ThCTL formation with i.n. vs i.s. APC transfer. **(F-G)** Experiment performed as in (A). Mice harvested 14-16hr post-transfer (pt) **(F)** Donor Nur77^{GFP} expression (i.n. vs i.v. APC) **(G)** Number of transferred APCs (i.n. vs i.v.). **(H-I)** Experiment performed as in (A). Mice were harvested 3-4 dpt. **(H)** Number of lung donor effectors with i.n. vs i.v. APC. **(I)** Donor lung ThCTL formation with i.n. vs i.v. APC. (B-C, F-G: n=8-11 per group pooled, 3 independent experiments. D-E, H-I: n=5-12 per group pooled, 2-4 independent experiments) Error bars represent s.e.m. Statistical significance determined by two-tailed, unpaired Student's t-test (* $P < 0.05$, ** $P < 0.01$ and *** $P < 0.001$). See also Fig S6.

Figure 6. DLN T_{FH} and spleen T_{FH} require local Ag presentation during the effector phase as shown by Ag delivery via i.n., i.s and i.v. routes (A) Experiment was performed as in Figure 5A. Mice were harvested 14-16hr post-transfer (pt) and donor cell Nur77^{GFP} expression was analyzed by flow cytometry in the DLN and spleen (i.n. vs i.s. APC). **(B-D)** Experiment was performed as in Figure 5A and mice were harvested 3-4 dpt. **(B)** Total numbers of DLN and spleen donor effectors recovered with i.n. vs i.s. APC transfer (n=5-12 per group pooled, 3-4 independent experiments). **(C)** DLN donor T_{FH} formation with i.n. vs i.s. APC transfer (n=5-10 per group pooled, 3 independent experiments) **(D)** Spleen donor T_{FH} formation with i.n. vs i.s. APC transfer (n=9-12 per group pooled, 4 independent experiments). **(E)** Experiment was performed as in

Figure 5A. Mice were harvested 14-16hr post-transfer (pt) and donor cell Nur77^{GFP} expression was analyzed by flow cytometry in the DLN and spleen (i.n. vs i.v. APC). **(F-H)** Experiment was performed as in Figure 5A. Mice were harvested 3-4 dpt. **(F)** Numbers of donor effectors in the DLN and spleen when APC were transferred i.n. vs i.v. (n=5-11 per group pooled, 2-3 independent experiments). **(G)** Donor T_{FH} formation in the DLN when APC were transferred i.n. vs i.v. (n=5-11 per group pooled, 2-3 independent experiments). **(H)** Donor T_{FH} formation in the spleen when APC were transferred i.n. vs i.v. (n=5-11 per group pooled, 2-3 independent experiments). Error bars represent s.e.m. Statistical significance determined by two-tailed, unpaired Student's t-test (* $P < 0.05$, ** $P < 0.01$ and *** $P < 0.001$). See also Figure S6.

MATERIALS AND METHODS

Mice

C57Bl/6 (B6), B6.CD45.1, B6.Thy1.1, B6.Nr4a1^{eGFP} (Nur77^{GFP}), B6.CD80/CD86 KO and B6.MHC II^{-} were obtained from the Jackson Laboratory. B6.TCRα/β KO mice were obtained from Dr. Raymond Welsh (UMMS). Y-linked B6.OT-II mice were obtained from Linda Bradley (The Scripps Research Institute, La Jolla, CA) and were originally published by Frank Carbone's group (Barnden et al., 1998) and were bred and maintained at the UMMS animal facility. BALB/c.HNT were obtained from David Lo (Scott et al., 1994) (The Scripps Research Institute, La Jolla, CA) originally and have been bred and maintained at the UMMS animal facility. Mice were at least 8 weeks old prior to use.

Virus stocks and infections

Influenza A viruses (IAV) A/Puerto Rico/8/34 (PR8), originally from St. Jude Children's Hospital, and A/PR8-OVA$_{II}$, kindly provided by Dr. Peter Doherty, were grown and maintained at the Trudeau Institute. Mice were anesthetized with isoflurane (Piramal Healthcare) or with Ketamine/Xylazine (at a dose of 25/2.5mg/kg by i.p. injection) and were infected intranasally with influenza virus corresponding to a 0.2-0.3 LD$_{50}$ dose of IAV in 50 uL of PBS.

Bone marrow chimera mice generation

Host mice for bone marrow chimeras were lethally irradiated with 2 doses of 570 rads, 3 hours apart. Bone marrow was isolated from the femurs and tibia of donor mice. The bone marrow was T cell depleted (using CD90.2 magnetic beads from Miltenyi) and adoptively transferred into lethally irradiated host mice by tail-vein i.v. injections. Bone marrow was transferred at a 1:1 or 1:2 donor:host mice ratio. Mice were allowed to recover and reconstitute for at least 6 weeks prior

759 to use during which they were treated with antibiotics (0.63mg/ml Sulfadiazine and 0.13mg/mL
760 Trimethoprim) added to their drinking water. Reconstitution was confirmed by flow cytometry of
761 peripheral blood before use and again in all tissues harvested when the mice were used in
762 experiments.

763 ***In vivo* day 6 effector generation and transfer/*in vitro* culture**

764 *In vivo* generated 6d CD4 T cell effectors were routinely obtained as described previously (Bautista
765 et al., 2016). Briefly, cells from lymph nodes and spleens of naïve OT-II or HNT transgenic mice
766 were enriched for naïve cells by percoll gradients and CD4 T cells isolated by CD4 positive
767 selection (Miltenyi Biotec) or using a CD4 naïve positive selection kit (Miltenyi Biotec). Naïve
768 CD4 T cells were adoptively transferred into mice (1st hosts), which were then infected with IAV
769 (PR8 or PR8-OVA_{II}). On day 6 post infection, the lung draining lymph nodes (DLN) and spleens
770 were harvested and donor T cells were isolated using MACS (Miltenyi Biotec) based on their
771 congenic marker (CD90.1). Immediately after isolation, the *in vivo* generated 1-2x10^6 6d CD4
772 effectors were adoptively transferred intravenously (i.v.) into host mice (2nd hosts).

773 *In vivo* generated 6d CD4 effectors were also cultured *in vitro* for 2 days by stimulating with plate
774 bound anti-CD3 (2C11, 0.5ug/ml) or anti-CD3 and anti-CD28 (37.51, 20ug/mL) in T cell media
775 (RPMI 1640 supplemented with 7.5% fetal bovine serum, 2mM L-glutamine, 50 uM 2-
776 mercaptoethanol, 100 IU penicillin, 100 ug/ml streptomycin and 10mM HEPES).

777 ***In vitro* APC culture and activation**

778 BMDC (bone marrow derived dendritic cells) (Bautista et al., 2016; Brahmakshatriya et al., 2017)
779 and activated B cell (Bautista et al., 2016) generation was done as described previously. Briefly,
780 bone marrow cells were flushed from femurs and tibia of mice and cultured *in vitro* with 10ng/mL

GMCSF (Biolegend). After 7 days, cells were harvested and enriched for dendritic cells with CD11c positive selection (Miltenyi Biotec). Dendritic cells were then matured with 10ug/mL Poly I:C (InVivoGen) overnight before use. Activated B cells were generated by isolating T depleted splenocytes using CD90.2 negative selection (Miltenyi Biotec) and culturing these *in vitro* for 2 days with 10ng/mL LPS and 10ng/mL dextran sulfate.

In vivo APC delivery

To deliver Ag/APC (BMDC or activated B cells), APC were pulsed with 10µM $OVA_{323–339}$ (OVA_{II}) peptide (New England Peptide) or no peptide as a negative control (unpulsed APC) for 1 hour at 37°C with shaking. APC were washed and administered either intravenously (i.v.) in 200uL PBS, intranasally (i.n.) in 50uL PBS, or intrasplenically (i.s.) in 10uL PBS. 0.25-1x10^6 BMDC or 1x10^6 B cells were transferred i.v., 0.5-2x10^6 BMDC or 1-2x10^6 B cells were transferred i.n. and 0.5-1x10^6 B cells were transferred i.s.

For intrasplenic transfer of APC, the animal was initially anaesthetized at 2.5%, then maintained at 1.5 – 1.75% isoflurane. Animal's hair was clipped from the hip to mid chest on the animal's left side. The area was sterilized and bupivacaine 1mg/kg was subcutaneously injected at the proposed incision site. Just below the last rib, using a pair of forceps, a 2 mm area of skin was held up and away from the body cavity and a 6-8mm incision was made by blunt dissection. PBS soaked cotton tipped applicators were used to lift the spleen out and hold in place. A 25µl Hamilton syringe with a 31-gauge Hamilton needle was used to inject the cells into the spleen. Sterile PBS was drawn into the syringe 3 times prior to the cells being drawn up. The syringe was held in a vertical position to the center of the spleen. The center of the top of spleen was penetrated by the needle at a depth of 2mm. The plunger was pushed slowly over a period of 10 seconds, and then the needle was left in the spleen for an additional 10 seconds. Using the cotton tipped applicators, the spleen was

placed back into the abdominal cavity. Muscle and skin layers were sutured closed. Upon completion of the surgery, meloxicam SR 4.0 mg/kg was administered subcutaneously over the right flank.

T cell functional assays

In vivo and *in vitro* cytotoxicity was performed as previously described (Marshall et al., 2016). Briefly, for *in vivo* cytotoxicity, T depleted splenocytes were stained with either 1uM or 0.4uM of CFSE denoting target (0.4uM) or bystander (1uM) cells. Target cells were pulsed with OVA_{II} peptide for 1 hour at 37°C. Both populations were washed twice in PBS and adoptively transferred into host mice. 18 hours later, the spleens of host mice were harvested and the number of target and bystander cells were quantified by flow cytometry. Specific killing was calculated as: 100 x (1- (live targets/live bystanders)) normalized to the ratio found in control mice. For *in vitro* cytotoxicity, targets were activated B cells that were labeled as above using CellTrace Violet (Invitrogen). Effectors and targets were co-cultured in 96 U bottom plates in T cell medium at 37°C 5% CO_2 for 4 hours. Plates were washed and stained for cell viability using Annexin V and 7-AAD (Invitrogen) or live/dead amine dyes (Invitrogen). Ag specific cytotoxicity was calculated as: 100 x (1- (live targets/live bystanders)) normalized to the ratio found in control wells with no effector cells. T cell degranulation and cytokine production was measured by *ex vivo* stimulation with plate bound 0.5ug/mL anti-CD3 and 20ug/mL anti-CD28 or with 10ng/mL PMA and 500ng/mL Ionomycin for 4 hours at 37°C, 5% CO_2 with brefeldin A (10ug/ml). T cell degranulation was also measured simultaneously with the addition of anti-CD107a PE (Biolegend, 1:200), and monensin (BD GolgiStop, according to manufacturer's protocol) at the beginning of the culture. Cells were harvested and stained for intracellular cytokines.

Flow cytometry

Cells were harvested and passed through a 70uM nylon mesh, washed, and stained in FACS buffer [0.5% Bovine Serum Albumin, 0.01% sodium azide (Sigma-Aldrich) in PBS]. Cells were blocked with anti-FcR (2.4G2) and then stained with amine reactive viability dyes to exclude dead cells (Invitrogen). Surface antigens were stained with fluorochrome conjugated antibodies. Antibodies used: anti- CD4 (GK1.5), CD19 (6D5), CD44 (IM7), CD90.1 (OX-7 and HIS51), CD95 (Fas, Jo2), CD107a (1D4B), CD150 (SLAM, TC15-12F12.2), CD183 (CXCR3, CXCR3-173), CD185 (CXCR5, SPRCL5), CD186 (CXCR6, SA051D1), CD278 (ICOS, C398.4A), CD279 (PD1, 29F.1A12), CD335 (NKp46, 29A1.4), GL-7, IgD (11-26c), NK1.1 (PK136), and NKG2A/C/E (20d5). Binding to P-selectin was measured by incubating with P-selectin IgG Fusion protein (BD Bioscience), washed and detected with fluorochrome conjugated secondary goat anti-human antibodies (Jackson ImmunoResearch). HA reactivity was detected using HA conjugated to FITC. Following surface staining, cells were fixed with 2% paraformaldehyde (Sigma-Aldrich). For intracellular staining of cytokines, cells were first surface stained then fixed with 4% paraformaldehyde for 20 min, washed, and permeabilized with 0.1% saponin buffer (1% FBS, 0.1%NaN_3 and 0.1% saponin in PBS, (Sigma-Aldrich) for 15 mins. Subsequent staining for cytokines using the following antibodies: anti-IFNγ (XMG1.2), anti- TNFα (MP6-XT22). IL-21 was detected using IL-21RFc (R&D systems), washed and detected with fluorochrome conjugated secondary goat anti-human antibodies (Jackson ImmunoResearch). GzmB was stained intracellulary directly *ex vivo* using anti-GzmB (GB11). For Bcl-6 staining, cells were first surface stained then fixed and permeabilized using the FoxP3 fix/perm kit (eBioscience) following manufacturer's protocol and stained with anti-Bcl-6 (K112-91). Antibodies were obtained from

eBioscience, Biolegend, or BD Bioscience. Stained cells were acquired on an LSRII flow cytometer (BD) and analyzed using FlowJo analysis software.

Statistics

Unpaired, two-tailed, Students t-test was used to assess statistical significance between the means of two groups, with $P < 0.05$ considered significant. Analysis was done using Prism (Graphpad) software. Error bars in the figures represent the standard error of the mean. Significance in the figures are indicated as * $P < 0.05$, ** $P < 0.01$ and *** $P < 0.001$. Expression levels of different markers analyzed by flow cytometry are shown as MFI (Median Fluorescence Intensity) or nMFI (normalized MFI). To correct for batch effects while pooling data from different experiments, we normalized MFI by dividing each data point within an experiment by the average MFI of the control group from that experiment. nMFI = MFI/(average MFI of the control group)

Study approval

Experimental animal procedures were done in accordance with UMMS Animal Care and Use Committee guidelines that meet IACUC guidelines.

REFERENCES

Allie, S.R., Bradley, J.E., Mudunuru, U., Schultz, M.D., Graf, B.A., Lund, F.E., and Randall, T.D. (2019). The establishment of resident memory B cells in the lung requires local antigen encounter. Nat Immunol *20*, 97-108.

Au-Yeung, B.B., Zikherman, J., Mueller, J.L., Ashouri, J.F., Matloubian, M., Cheng, D.A., Chen, Y., Shokat, K.M., and Weiss, A. (2014). A sharp T-cell antigen receptor signaling threshold for T-cell proliferation. Proc Natl Acad Sci U S A *111*, E3679-3688.

Barnden, M.J., Allison, J., Heath, W.R., and Carbone, F.R. (1998). Defective TCR expression in transgenic mice constructed using cDNA-based alpha- and beta-chain genes under the control of heterologous regulatory elements. Immunol Cell Biol *76*, 34-40.

Baumjohann, D., Preite, S., Reboldi, A., Ronchi, F., Ansel, K.M., Lanzavecchia, A., and Sallusto, F. (2013). Persistent antigen and germinal center B cells sustain T follicular helper cell responses and phenotype. Immunity *38*, 596-605.

Bautista, B.L., Devarajan, P., McKinstry, K.K., Strutt, T.M., Vong, A.M., Jones, M.C., Kuang, Y., Mott, D., and Swain, S.L. (2016). Short-Lived Antigen Recognition but Not Viral Infection at a Defined Checkpoint Programs Effector CD4 T Cells To Become Protective Memory. J Immunol *197*, 3936-3949.

Beura, L.K., Wijeyesinghe, S., Thompson, E.A., Macchietto, M.G., Rosato, P.C., Pierson, M.J., Schenkel, J.M., Mitchell, J.S., Vezys, V., Fife, B.T., *et al.* (2018). T Cells in Nonlymphoid Tissues Give Rise to Lymph-Node-Resident Memory T Cells. Immunity *48*, 327-338 e325.

Botta, D., Fuller, M.J., Marquez-Lago, T.T., Bachus, H., Bradley, J.E., Weinmann, A.S., Zajac, A.J., Randall, T.D., Lund, F.E., Leon, B., and Ballesteros-Tato, A. (2017). Dynamic regulation of T follicular regulatory cell responses by interleukin 2 during influenza infection. Nat Immunol *18*, 1249-1260.

Brahmakshatriya, V., Kuang, Y., Devarajan, P., Xia, J., Zhang, W., Vong, A.M., and Swain, S.L. (2017). IL-6 Production by TLR-Activated APC Broadly Enhances Aged Cognate CD4 Helper and B Cell Antibody Responses In Vivo. J Immunol *198*, 2819-2833.

Broadley, I., Pera, A., Morrow, G., Davies, K.A., and Kern, F. (2017). Expansions of Cytotoxic CD4(+)CD28(-) T Cells Drive Excess Cardiovascular Mortality in Rheumatoid Arthritis and Other Chronic Inflammatory Conditions and Are Triggered by CMV Infection. Front Immunol *8*, 195.

Brown, D.M., Lee, S., Garcia-Hernandez Mde, L., and Swain, S.L. (2012). Multifunctional CD4 cells expressing gamma interferon and perforin mediate protection against lethal influenza virus infection. J Virol *86*, 6792-6803.

Crotty, S. (2019). T Follicular Helper Cell Biology: A Decade of Discovery and Diseases. Immunity *50*, 1132-1148.

Deenick, E.K., Chan, A., Ma, C.S., Gatto, D., Schwartzberg, P.L., Brink, R., and Tangye, S.G. (2010). Follicular helper T cell differentiation requires continuous antigen presentation that is independent of unique B cell signaling. Immunity *33*, 241-253.

Deenick, E.K., Ma, C.S., Brink, R., and Tangye, S.G. (2011). Regulation of T follicular helper cell formation and function by antigen presenting cells. Curr Opin Immunol *23*, 111-118.

Devarajan, P., Bautista, B., Vong, A.M., McKinstry, K.K., Strutt, T.M., and Swain, S.L. (2016). New Insights into the Generation of CD4 Memory May Shape Future Vaccine Strategies for Influenza. Front Immunol *7*, 136.

Devarajan, P., Jones, M.C., Kugler-Umana, O., Vong, A.M., Xia, J., and Swain, S.L. (2018). Pathogen Recognition by CD4 Effectors Drives Key Effector and Most Memory Cell Generation Against Respiratory Virus. Front Immunol *9*, 596.

Dubey, C., and Croft, M. (1996). Accessory molecule regulation of naive CD4 T cell activation. Immunol Res *15*, 114-125.

Fazilleau, N., McHeyzer-Williams, L.J., Rosen, H., and McHeyzer-Williams, M.G. (2009). The function of follicular helper T cells is regulated by the strength of T cell antigen receptor binding. Nat Immunol *10*, 375-384.

Gensous, N., Charrier, M., Duluc, D., Contin-Bordes, C., Truchetet, M.E., Lazaro, E., Duffau, P., Blanco, P., and Richez, C. (2018). T Follicular Helper Cells in Autoimmune Disorders. Front Immunol *9*, 1637.

Inoue, T., Moran, I., Shinnakasu, R., Phan, T.G., and Kurosaki, T. (2018). Generation of memory B cells and their reactivation. Immunol Rev *283*, 138-149.

Jelley-Gibbs, D.M., Brown, D.M., Dibble, J.P., Haynes, L., Eaton, S.M., and Swain, S.L. (2005). Unexpected prolonged presentation of influenza antigens promotes CD4 T cell memory generation. J Exp Med *202*, 697-706.

Juno, J.A., van Bockel, D., Kent, S.J., Kelleher, A.D., Zaunders, J.J., and Munier, C.M. (2017). Cytotoxic CD4 T Cells-Friend or Foe during Viral Infection? Front Immunol *8*, 19.

Khan, T.N., Mooster, J.L., Kilgore, A.M., Osborn, J.F., and Nolz, J.C. (2016). Local antigen in nonlymphoid tissue promotes resident memory CD8+ T cell formation during viral infection. J Exp Med *213*, 951-966.

Koutsakos, M., McWilliam, H.E.G., Aktepe, T.E., Fritzlar, S., Illing, P.T., Mifsud, N.A., Purcell, A.W., Rockman, S., Reading, P.C., Vivian, J.P., *et al.* (2019a). Downregulation of MHC Class I Expression by Influenza A and B Viruses. Front Immunol *10*, 1158.

Koutsakos, M., Nguyen, T.H.O., and Kedzierska, K. (2019b). With a Little Help from T Follicular Helper Friends: Humoral Immunity to Influenza Vaccination. J Immunol *202*, 360-367.

Krishnaswamy, J.K., Alsen, S., Yrlid, U., Eisenbarth, S.C., and Williams, A. (2018). Determination of T Follicular Helper Cell Fate by Dendritic Cells. Front Immunol *9*, 2169.

Lee, J.Y., Skon, C.N., Lee, Y.J., Oh, S., Taylor, J.J., Malhotra, D., Jenkins, M.K., Rosenfeld, M.G., Hogquist, K.A., and Jameson, S.C. (2015). The transcription factor KLF2 restrains CD4(+) T follicular helper cell differentiation. Immunity *42*, 252-264.

Lewis, S.M., Williams, A., and Eisenbarth, S.C. (2019). Structure and function of the immune system in the spleen. Sci Immunol *4*.

Linterman, M.A., Denton, A.E., Divekar, D.P., Zvetkova, I., Kane, L., Ferreira, C., Veldhoen, M., Clare, S., Dougan, G., Espeli, M., and Smith, K.G. (2014). CD28 expression is required after T cell priming for helper T cell responses and protective immunity to infection. Elife *3*.

Malhotra, D., Fletcher, A.L., and Turley, S.J. (2013). Stromal and hematopoietic cells in secondary lymphoid organs: partners in immunity. Immunol Rev *251*, 160-176.

Marshall, N.B., and Swain, S.L. (2011). Cytotoxic CD4 T cells in antiviral immunity. J Biomed Biotechnol *2011*, 954602.

Marshall, N.B., Vong, A.M., Devarajan, P., Brauner, M.D., Kuang, Y., Nayar, R., Schutten, E.A., Castonguay, C.H., Berg, L.J., Nutt, S.L., and Swain, S.L. (2016). NKG2C/E Marks the Unique Cytotoxic CD4 T Cell Subset, ThCTL, Generated by Influenza Infection. J Immunol.

McKinstry, K.K., Strutt, T.M., Bautista, B., Zhang, W., Kuang, Y., Cooper, A.M., and Swain, S.L. (2014). Effector CD4 T-cell transition to memory requires late cognate interactions that induce autocrine IL-2. Nat Commun *5*, 5377.

McKinstry, K.K., Strutt, T.M., Kuang, Y., Brown, D.M., Sell, S., Dutton, R.W., and Swain, S.L. (2012). Memory CD4+ T cells protect against influenza through multiple synergizing mechanisms. J Clin Invest *122*, 2847-2856.

McMaster, S.R., Wein, A.N., Dunbar, P.R., Hayward, S.L., Cartwright, E.K., Denning, T.L., and Kohlmeier, J.E. (2018). Pulmonary antigen encounter regulates the establishment of tissue-resident CD8 memory T cells in the lung airways and parenchyma. Mucosal Immunol *11*, 1071-1078.

Melssen, M., and Slingluff, C.L., Jr. (2017). Vaccines targeting helper T cells for cancer immunotherapy. Curr Opin Immunol *47*, 85-92.

Moran, A.E., Holzapfel, K.L., Xing, Y., Cunningham, N.R., Maltzman, J.S., Punt, J., and Hogquist, K.A. (2011). T cell receptor signal strength in Treg and iNKT cell development demonstrated by a novel fluorescent reporter mouse. J Exp Med *208*, 1279-1289.

Moyer, T.J., Kato, Y., Abraham, W., Chang, J.Y.H., Kulp, D.W., Watson, N., Turner, H.L., Menis, S., Abbott, R.K., Bhiman, J.N., *et al.* (2020). Engineered immunogen binding to alum adjuvant enhances humoral immunity. Nat Med *26*, 430-440.

Moyer, T.J., Zmolek, A.C., and Irvine, D.J. (2016). Beyond antigens and adjuvants: formulating future vaccines. J Clin Invest *126*, 799-808.

Muraro, E., Merlo, A., Martorelli, D., Cangemi, M., Dalla Santa, S., Dolcetti, R., and Rosato, A. (2017). Fighting Viral Infections and Virus-Driven Tumors with Cytotoxic CD4(+) T Cells. Front Immunol *8*, 197.

Phetsouphanh, C., Pillai, S., and Zaunders, J.J. (2017). Editorial: Cytotoxic CD4+ T Cells in Viral Infections. Front Immunol *8*, 1729.

Schenkel, J.M., Fraser, K.A., and Masopust, D. (2014). Cutting edge: resident memory CD8 T cells occupy frontline niches in secondary lymphoid organs. J Immunol *192*, 2961-2964.

Scott, B., Liblau, R., Degermann, S., Marconi, L.A., Ogata, L., Caton, A.J., McDevitt, H.O., and Lo, D. (1994). A role for non-MHC genetic polymorphism in susceptibility to spontaneous autoimmunity. Immunity *1*, 73-83.

Serroukh, Y., Gu-Trantien, C., Hooshiar Kashani, B., Defrance, M., Vu Manh, T.P., Azouz, A., Detavernier, A., Hoyois, A., Das, J., Bizet, M., *et al.* (2018). The transcription factors Runx3 and ThPOK cross-regulate acquisition of cytotoxic function by human Th1 lymphocytes. Elife *7*.

Swain, S.L., McKinstry, K.K., and Strutt, T.M. (2012). Expanding roles for CD4(+) T cells in immunity to viruses. Nat Rev Immunol *12*, 136-148.

Takamura, S., Yagi, H., Hakata, Y., Motozono, C., McMaster, S.R., Masumoto, T., Fujisawa, M., Chikaishi, T., Komeda, J., Itoh, J., *et al.* (2016). Specific niches for lung-resident memory CD8+ T cells at the site of tissue regeneration enable CD69-independent maintenance. J Exp Med *213*, 3057-3073.

Tam, H.H., Melo, M.B., Kang, M., Pelet, J.M., Ruda, V.M., Foley, M.H., Hu, J.K., Kumari, S., Crampton, J., Baldeon, A.D., *et al.* (2016). Sustained antigen availability during germinal center initiation enhances antibody responses to vaccination. Proc Natl Acad Sci U S A *113*, E6639-E6648.

van de Berg, P.J., van Leeuwen, E.M., ten Berge, I.J., and van Lier, R. (2008). Cytotoxic human CD4(+) T cells. Curr Opin Immunol *20*, 339-343.

Vinuesa, C.G., Linterman, M.A., Yu, D., and MacLennan, I.C. (2016). Follicular Helper T Cells. Annu Rev Immunol *34*, 335-368.

Watts, T.H. (2010). Staying alive: T cell costimulation, CD28, and Bcl-xL. J Immunol *185*, 3785-3787.